

**NEUTRON STAR STRUCTURE AND  
THE EQUATION OF STATE**

J. M. LATTIMER AND M. PRAKASH

Department of Physics and Astronomy, State University of New York at Stony Brook  
Stony Brook, NY 11974-3800

Received \_\_\_\_\_; accepted \_\_\_\_\_

## ABSTRACT

The structure of neutron stars is considered from theoretical and observational perspectives. We demonstrate an important aspect of neutron star structure: the neutron star radius is primarily determined by the behavior of the pressure of matter in the vicinity of nuclear matter equilibrium density. In the event that extreme softening does not occur at these densities, the radius is virtually independent of the mass and is determined by the magnitude of the pressure. For equations of state with extreme softening, or those that are self-bound, the radius is more sensitive to the mass. Our results show that in the absence of extreme softening, a measurement of the radius of a neutron star more accurate than about 1 km will usefully constrain the equation of state. We also show that the pressure near nuclear matter density is primarily a function of the density dependence of the nuclear symmetry energy, while the nuclear incompressibility and skewness parameters play secondary roles.

In addition, we show that the moment of inertia and the binding energy of neutron stars, for a large class of equations of state, are nearly universal functions of the star's compactness. These features can be understood by considering two analytic, yet realistic, solutions of Einstein's equations, due, respectively, to Buchdahl and Tolman. We deduce useful approximations for the fraction of the moment of inertia residing in the crust, which is a function of the stellar compactness and, in addition, the pressure at the core-crust interface.

*Subject headings:* structure of stars – equation of state – stars: interiors – stars: neutron

## 1. INTRODUCTION

The theoretical study of the structure of neutron stars is crucial if new observations of masses and radii are to lead to effective constraints on the equation of state (EOS) of dense matter. This study becomes ever more important as laboratory studies may be on the verge of yielding evidence about the composition and stiffness of matter beyond the nuclear equilibrium density  $\rho_s \cong 2.7 \cdot 10^{14} \text{ g cm}^{-3}$ . Rhoades & Ruffini (1974) demonstrated that the assumption of causality beyond a fiducial density  $\rho_f$  sets an upper limit to the maximum mass of a neutron star:  $4.2\sqrt{\rho_s/\rho_f} M_\odot$ . However, theoretical studies of dense matter have considerable uncertainty in the high-density behavior of the EOS largely because of the poorly constrained many-body interactions. These uncertainties have prevented a firm prediction of the maximum mass of a beta-stable neutron star.

To date, several accurate mass determinations of neutron stars are available from radio binary pulsars (Thorsett & Chakrabarty 1998), and they all lie in a narrow range ( $1.25 - 1.44 M_\odot$ ). One neutron star in an X-ray binary, Cyg X-2, has an estimated mass of  $1.8 \pm 0.2 M_\odot$  (Orosz & Kuulkers 1999), but this determination is not as clean as for a radio binary. Another X-ray binary, Vela X-1, has a reported mass around  $1.9 M_\odot$  (van Kerkwijk et al. 1995a), although Stickland et al. (1997) argue it to be about  $1.4 M_\odot$ . A third object, the eclipsing X-ray binary 4U 1700-37, apparently contains an object with a mass of  $1.8 \pm 0.4 M_\odot$  (Heap & Corcoran 1992), but Brown, Weingartner & Wijers (1996) have argued that since this source does not pulse and has a relatively hard X-ray spectrum, it may contain a low-mass black hole instead. It would not be surprising if neutron stars in X-ray binaries had larger masses than those in radio binaries, since the latter have presumably accreted relatively little mass since their formation. Alternatively, Cyg X-2 could be the first of a new and rarer population of neutron stars formed with high masses which could originate from more massive, rarer, supernovae. If the high masses for Cyg X-2

or Vela X-1 are confirmed, significant constraints on the equation of state would be realized.

On the other hand, there is a practical, albeit theoretical, lower mass limit for neutron stars, about  $1.1 - 1.2 M_{\odot}$ , which follows from the minimum mass of a protonneutron star. This is estimated by examining a lepton-rich configuration with a low-entropy inner core of  $\sim 0.6 M_{\odot}$  and a high-entropy envelope (Goussard, Haensel & Zdunik 1998). This argument is in general agreement with the theoretical result of supernova calculations, in which the inner homologous collapsing core material comprises at least  $1 M_{\odot}$ .

Although accurate masses of several neutron stars are available, a precise measurement of the radius does not yet exist. Lattimer et al. (1990) (see also Glendenning 1992) have shown that the causality constraint can be used to set a lower limit to the radius:  $R \gtrsim 3.04GM/Rc^2$ . For a  $1.4 M_{\odot}$  star, this is about 4.5 km.

Estimates of neutron star radii from observations have given a wide range of results. Perhaps the most reliable estimates stem from observations of thermal emissions from neutron star surfaces, which yield values of the so-called “radiation radius”

$$R_{\infty} = R/\sqrt{1 - 2GM/Rc^2}, \quad (1)$$

a quantity resulting from redshifting the stars luminosity and temperature. A given value of  $R_{\infty}$  implies that  $R < R_{\infty}$  and  $M < 0.13(R_{\infty}/\text{km}) M_{\odot}$ . Thus, a  $1.4 M_{\odot}$  neutron star requires  $R_{\infty} > 10.75$  km. Those pulsars with at least some suspected thermal radiation generically yield effective values of  $R_{\infty}$  so small that it is believed that a significant part of the radiation originates from polar hot spots rather than from the surface as a whole. For example, Golden & Shearer (1999) found that upper limits to the unpulsed emission from Geminga, coupled with a parallactic distance of 160 pc, yielded values of  $R_{\infty} \lesssim 9.5$  km for a blackbody source and  $R_{\infty} \lesssim 10$  km for a magnetized H atmosphere. Similarly, Schulz (1999) estimated emission radii of less than 5 km, assuming a blackbody for eight low mass X-ray binaries.

Other attempts to deduce a radius include analyses (Titarchuk 1994) of X-ray bursts from sources 4U 1705-44 and 4U 1820-30 which implied rather small values,  $9.5 < R_\infty < 14$  km. Recently, Rutledge et al. (1999) found that thermal emission from neutron stars of a canonical 10 km radius was indicated by the interburst emission. However, the modeling of the photospheric expansion and touchdown on the neutron star surface requires a model dependent relationship between the color and effective temperatures.

Absorption lines in X-ray spectra have also been investigated (Inoue 1992) with a view to deducing the neutron star radius. Candidates for the matter producing the absorption lines are either the accreted matter from the companion star or the products of nuclear burning in the bursts. In the former case, the most plausible element is thought to be Fe, in which case the relation  $R \approx 3.2GM/c^2$ , only slightly larger than the minimum possible value based upon causality (Lattimer et al. 1990; Glendenning 1992) is inferred. In the latter case, plausible candidates are Ti and Cr, and larger values of the radius would be obtained. In both cases, serious difficulties remain in interpreting the large line widths, of order 100–500 eV, in the  $4.1 \pm 0.1$  keV line observed from many sources.

A first attempt at using light curves and pulse fractions from pulsars to explore the  $M - R$  relation suggested relatively large radii, of order 15 km (Page 1995). However, this method, which assumed dipolar magnetic fields, was unable to satisfactorily reconcile the calculated magnitudes of the pulse fractions and the shapes of the light curves with observations.

The discovery of Quasi-Periodic Oscillations (QPOs) from X-ray emitting neutron stars in binaries provides a possible way of limiting neutron star masses and radii. These oscillations are manifested as quasi-periodic X-ray emissions, with frequencies ranging from tens to over 1200 Hz. Some QPOs show multiple frequencies, in particular, two frequencies  $\nu_1$  and  $\nu_2$  at several hundred Hz. These frequencies are not constant, but tend

to both increase with time until the signal ultimately weakens and disappears. In the beat frequency model (Alpar & Shaham 1985, Psaltis et al. 1998), the highest frequency  $\nu_2$  is associated with the Keplerian frequency  $\nu_K$  of inhomogeneities or blobs in an accretion disc. The largest such frequency measured to date is  $\nu_{max} = 1230$  Hz. However, general relativity predicts the existence of a maximum orbital frequency, since the inner edge of an accretion disc must remain outside of the innermost stable circular orbit, located at a radius of  $r_s = 6GM/c^2$  in the absence of rotation. This corresponds to a Keplerian orbital frequency of  $\nu_s = \sqrt{GM/r_s^3}/2\pi$  if the star is non-rotating. Equating  $\nu_{max}$  with  $\nu_s$ , and since  $R < r_s$ , one deduces

$$M \lesssim 1.78 M_\odot; \quad R \lesssim 8.86(M/M_\odot) \text{ km.} \quad (2)$$

Corrections due to stellar rotation are straightforward to deduce and produce small changes in these limits (Psaltis et al. 1998). The lower frequency  $\nu_1$  is associated with a beat frequency between  $\nu_2$  and the spin frequency of the star. This spin frequency is large enough, of order 250-350 Hz, to alter the metric from a Schwarzschild geometry, and increases the theoretical mass limit in equation (2) to about  $2.1 M_\odot$  (Psaltis et al. 1998). This remains strictly an upper limit, however, unless further observations support the interpretation that  $\nu_{max}$  is associated with orbits at precisely the innermost stable orbit.

If the frequency  $\nu_2 - \nu_1$  is to be associated with the spin of the neutron star, it should remain constant in time. However, recent observations reveal that it changes with time in a given source. Osherovich & Titarchuk (1999) proposed a model in which  $\nu_1$  is the Keplerian frequency and  $\nu_2$  is a hybrid frequency of the Keplerian oscillator under the influence of a magnetospheric Coriolis force. In this model, the frequencies are related to the neutron star spin frequency  $\nu$  by

$$\nu_2 = \sqrt{\nu_1^2 + (\nu/2\pi)^2}. \quad (3)$$

Osherovich & Titarchuk argue that this relation fits the observed variations of  $\nu_2$  and  $\nu_1$  in several QPOs. The Keplerian frequency in Osherovich & Titarchuk's model, being

associated with the lower frequency  $\nu_1$ , however, is at most 800 Hz, leading to an upper mass limit that is nearly  $3 M_\odot$  and is therefore of little practical use to limit either the star’s mass or radius.

An alternative model, proposed by Stella & Vietri (1999), associates  $\nu_2$  with the Keplerian frequency of the inner edge of the disc,  $\nu_K$ , and  $\nu_2 - \nu_1$  with the precession frequency of the periastron of slightly eccentric orbiting blobs at radius  $r$  in the accretion disc. In a Schwarzschild geometry,  $\nu_1 = \nu_K \sqrt{1 - 6GM/r c^2}$ . Note that  $(\nu_K - \nu_1)^{-1}$  is the timescale that an orbiting blob recovers its original orientation relative to the neutron star and the Earth, so that variations in flux are expected to be observed at both frequencies  $\nu_K$  and  $\nu_K - \nu_1$ . Presumably, even eccentricities of order  $10^{-4}$  lead to observable effects. This model predicts that

$$\nu_1/\nu_2 = 1 - \sqrt{1 - 6(GM\nu_2)^{2/3}/c^2}, \quad (4)$$

a relation that depends only upon  $M$ . Equation (4) can also fit observations of QPOs, but only if  $1.9 \lesssim M/M_\odot \lesssim 2.1$ . This result is not very sensitive to complicating effects due to stellar rotation: the Lense-Thirring effect and oblateness. This mechanism only depends on gravitometric effects, and may apply also to accreting black hole systems (Stella, Vietri & Morsink 1999).

Prospects for a radius determination have improved in recent years with the discovery of a class of isolated, non-pulsing, neutron stars. The first of these is the nearby object RX J185635-3754, initially discovered in X-rays (Walter, Wolk & Neuhauser 1996) and confirmed with the Hubble Space Telescope (Walter & Matthews 1997). The observed X-rays, from the ROSAT satellite, are consistent with blackbody emission with an effective temperature of about 57 eV and relatively little extinction. The fortuitous location of the star, in the foreground of the R CrA molecular cloud, coupled with the small levels of extinction, limits the distance to  $D < 120$  pc. The fact that the source is not observable

in radio and its lack of variability in X-rays implies that it is not a pulsar, unlike other identified radio-silent isolated neutron stars. This gives the hope that the observed radiation is not contaminated with non-thermal emission as in the case for pulsars.

The X-ray flux of RX J185635-3754, combined with a best-fit blackbody  $T_{eff} = 57$  eV, yields  $R_\infty \approx 7.3(D/120 \text{ pc})$  km. Such a value for  $R_\infty$ , even coupled with the maximum distance of 120 pc, is too small to be consistent with any neutron star with more than  $1 M_\odot$ . But the optical flux is about a factor of 4 brighter than what is predicted by the X-ray blackbody. The reconciliation the X-ray and optical fluxes through atmosphere modeling naively implies an increase in  $R_\infty$  of approximately  $4^{2/3} \cong 2.5$ . (This results since the X-ray flux is proportional to  $R_\infty^2 T_{eff}^4$ , while the optical flux is on the Rayleigh-Jeans tail of the spectrum and is hence proportional to  $R_\infty^2 T_{eff}$ . One seeks to enhance the predicted optical flux by 4 while keeping the X-ray flux fixed, as this is approximately equal to the total flux.) An et al. (2000) determined for non-magnetized heavy element atmospheres that  $R_\infty/D \cong 0.18 \pm 0.05 \text{ km pc}^{-1}$ , which is rough agreement with the above naive expectations. However, uncertainties in the atmospheric composition and the quality of the existing data precluded obtaining a more precise estimate of  $R_\infty/D$ . An et al. concluded, in agreement with expectations based upon the general results of Romani (1987) and Rajagopal, Romani & Miller (1997), that the predicted spectrum of a heavy element atmosphere, but not a light element atmosphere, was consistent with all the observations. This is in contrast to the conclusions of Pavlov et al. (1996), whose results for RX J185635-3754 implied that the observations in the optical and X-ray bands were incompatible with atmospheric modelling for both heavy element and light element non-magnetized atmospheres, unless the distance to this star is greater than the presumed maximum of 120 pc based upon the star's location in front of the R Cor Aus molecular cloud. Future prospects for determining the radius of this neutron star are discussed in §7.



Our objectives in this paper are 1) to demonstrate specifically how the accurate measurement of a neutron star radius would constrain the dense matter EOS, and 2) to provide general relationships for other structural quantities, such as the moment of inertia and the binding energy, that are relatively EOS-independent, and which could be used to constrain the neutron star mass and/or radius. We will examine a wide class of equations of state, including those that have extreme softening at high densities. In addition, we will examine analytic solutions to Einstein’s equations which shed light on the results we deduce empirically. In all cases, we will focus on non-rotating, non-magnetized neutron stars at zero temperature.

Lindblom (1992) had suggested that a series of mass and radius measurements would be necessary to accurately constrain the dense matter equation of state. His technique utilizes a numerical inversion of the neutron star structure equation. Our results instead suggest that important constraints on the EOS can be achieved with even a single radius measurement, if it is accurate enough, and that the quality of the constraint is not very sensitive to the mass. The fact that the range of accurately determined neutron star masses is so small, only about  $0.2 M_{\odot}$  to date, further implies that important constraints can be deduced without simultaneous mass-radius measurements. Of course, several measurements of neutron star masses and radii would greatly enhance the constraint on the equation of state.

In § 2, the equations of state selected in this paper are discussed. In § 3, the mass-radius relation for a sample of these equations of state are discussed. A quantitative relationship between the radii of normal neutron stars and the pressure of matter in the vicinity of  $n_s$  is empirically established and theoretically justified. In turn, how the matter’s pressure at these densities depends upon fundamental nuclear parameters is developed. In § 4, analytic solutions to the general relativistic equations of hydrostatic equilibrium are explored. These

lead to useful approximations for neutron star structure and which directly correlate other observables such as moments of inertia and binding energy to the mass and radius. It is believed that the distribution of the moment of inertia inside the star is crucial in the interpretation of glitches observed in the spin down of pulsars, so that measurements of the sizes and frequencies of glitches can constrain neutron star masses and radii (Link, Epstein & Lattimer 1999). In § 5, expressions for the fraction of moment of inertia contained within the stellar crust, as a function of mass, radius, and equation of state, are derived. In § 6, expressions for the binding energy are derived. § 7 contains a summary and outlook.

## 2. EQUATIONS OF STATE

The composition of a neutron star chiefly depends on the nature of strong interactions, which are not well understood in dense matter. Most models that have been investigated can be conveniently grouped into three broad categories: nonrelativistic potential models, relativistic field theoretical models, and relativistic Dirac-Brueckner-Hartree-Fock models. In each of these approaches, the presence of additional softening components such as hyperons, Bose condensates or quark matter, can be incorporated. Details of these approaches have been further considered in Lattimer et al. (1990) and Prakash et al. (1997). A representative sample, and some general attributes, including references and typical compositions, of equations of state employed in this paper are summarized in Table 1.

We have used four equations of state taken from Akmal & Pandharipande (1998). These are: AP1 (the AV18 potential), AP2 (the AV18 potential plus  $\delta v_b$  relativistic boost corrections), AP3 (the AV18 potential plus a three-body UIX potential), and AP4 (the AV18 potential plus the UIX potential plus the  $\delta v_b$  boost). Three equations of state from Müller & Serot (1996), labelled MS1–3, correspond to different choices of the parameters  $\xi$

and  $\zeta$  which determine the strength of the nonlinear vector and isovector interactions at high densities. The numerical values used are  $\xi = \zeta = 0$ ;  $\xi = 1.5, \zeta = 0.06$ ; and  $\xi = 1.5, \zeta = 0.02$ , respectively. Six EOSs from the phenomenological non-relativistic potential model of Prakash, Ainsworth & Lattimer (1988), labelled PAL1–6, were chosen, which have different choices of the symmetry energy parameter at the saturation density, its density dependence, and the bulk nuclear matter incompressibility parameter  $K_s$ . The incompressibilities of PAL1–5 were chosen to be  $K_s = 180$  or  $240$  MeV, but PAL6 has  $K_s = 120$  MeV. Three interactions from the field-theoretical model of Glendenning & Moszkowski (1991) are taken from their Table II; in order, they are denoted GM1–3. Two interactions from the field-theoretical model of Glendenning & Schaffner-Bielich (1999) correspond, in their notation, to GL78 with  $U_K(\rho_0) = -140$  MeV and TM1 with  $U_K = -185$  MeV. The labels denoting the other EOSs in Table I are identical to those in the original references.

The rationale for exploring a wide variety of EOSs, even some that are relatively outdated or in which systematic improvements are performed, is two-fold. First, it provides contrasts among widely different theoretical paradigms. Second, it illuminates general relationships that exist between the pressure-density relation and the macroscopic properties of the star such as the radius. For example, AP4 represents the most complete study to date of Akmal & Pandharipande (1998), in which many-body and special relativistic corrections are progressively incorporated into prior models, AP1–3. AP1–3 are included here because they represent different pressure-energy density-baryon density relations, and serve to reinforce correlations between neutron star structure and microscopic physics observed using alternative theoretical paradigms. Similarly, several different parameter sets for other EOSs are chosen.

In all cases, except for PS (Pandharipande & Smith 1975), the pressure is evaluated assuming zero temperature and beta equilibrium without trapped neutrinos. PS only

contains neutrons among the baryons, there being no charged components. We chose to include this EOS, despite the fact that it has been superseded by more sophisticated calculations by Pandharipande and coworkers, because it represents an extreme case producing large radii neutron stars.

The pressure-density relations for some of the selected EOSs are shown in Figure 1. There are two general classes of equations of state. First, *normal* equations of state have a pressure which vanishes as the density tends to zero. Second, *self-bound* equations of state have a pressure which vanishes at a significant finite density.

The best-known example of self-bound stars results from Witten’s (1984) conjecture (also see Fahri & Jaffe 1984, Haensel, Zdunik & Schaeffer 1986, Alcock & Olinto 1988, and Prakash et al. 1990) that strange quark matter is the ultimate ground state of matter. In this paper, the self-bound EOSs are represented by strange-quark matter models SQM1–3, using perturbative QCD and an MIT-type bag model, with parameter values given in Table 2. The existence of an energy ceiling equal to the baryon mass, 939 MeV, for zero pressure matter requires that the bag constant  $B \leq 94.92 \text{ MeV fm}^{-3}$ . This limiting value is chosen, together with zero strange quark mass and no interactions ( $\alpha_c = 0$ ), for the model SQM1. The other two models chosen, SQM2 and SQM3, have bag constants adjusted so that their energy ceilings are also 939 MeV.

For normal matter, the EOS is that of an interacting nucleon gas above a transition density of  $1/3$  to  $1/2 n_s$ . Below this density, the ground state of matter consists of heavy nuclei in equilibrium with a neutron-rich, low-density gas of nucleons. In general, a self-consistent evaluation of the equilibrium that exists below the transition density, and the evaluation of the transition density itself, has been carried out for only a few equations of state (e.g., Bethe, Pethick & Sutherland 1972, Negele & Vautherin 1974, Lattimer et al. 1985; Lattimer and Swesty 1990). We have therefore not plotted the pressure below

about  $0.1 \text{ MeV fm}^{-3}$  in Figure 1. For densities  $0.001 < n < 0.08 \text{ fm}^{-3}$  we employ the EOS of Negele & Vautherin (1974), while for densities  $n < 0.001 \text{ fm}^{-3}$  we employ the EOS of Bethe, Pethick & Sutherland (1972). However, for most of the purposes of this paper, the pressure in the region  $n < 0.1 \text{ fm}^{-3}$  is not relevant as it does not significantly affect the mass-radius relation or other global aspects of the star’s structure. Nevertheless, the value of the transition density, and the pressure there, are important ingredients for the determination of the size of the superfluid crust of a neutron star that is believed to be involved in the phenomenon of pulsar glitches (Link, Epstein & Lattimer 1999).

There are three significant features to note in Figure 1 for normal EOSs. First, there is a fairly wide range of predicted pressures for beta-stable matter in the density domain  $n_s/2 < n < 2n_s$ . For the EOSs displayed, the range of pressures covers about a factor of five, but this survey is by no means exhaustive. That such a wide range in pressures is found is somewhat surprising, given that each of the EOSs provides acceptable fits to experimentally-determined nuclear matter properties. Clearly, the extrapolation of the pressure from symmetric matter to nearly pure neutron matter is poorly constrained. Second, the *slopes* of the pressure curves are rather similar. A polytropic index of  $n \simeq 1$ , where  $P = Kn^{1+1/n}$ , is implied. Third, in the density domain below  $2n_s$ , the pressure-density relations seem to fall into two groups. The higher pressure group is primarily composed of relativistic field-theoretical models, while the lower pressure group is primarily composed of non-relativistic potential models. As we show in § 3, the pressure in the vicinity of  $n_s$  is mostly determined by the symmetry energy properties of the EOS, and it is significant that relativistic field-theoretical models generally have symmetry energies that increase proportionately to the density while potential models have much less steeply rising symmetry energies.

A few of the plotted normal EOSs have considerable softening at high densities,

especially PAL6, GS1, GS2, GM3, PS and PCL2. PAL6 has an abnormally small value of incompressibility ( $K_s = 120$  MeV). GS1 and GS2 have phase transitions to matter containing a kaon condensate, GM3 has a large population of hyperons appearing at high density, PS has a phase transition to a neutral pion condensate and a neutron solid, and PCL2 has a phase transition to a mixed phase containing strange quark matter. These EOSs can be regarded as representative of the many suggestions of the kinds of softening that could occur at high densities.

### 3. NEUTRON STAR RADII

Figure 2 displays the mass-radius relation for cold, catalyzed matter using these EOSs. The causality constraint described earlier and contours of  $R_\infty$  are also indicated in Figure 2. With the exception of model GS1, the EOSs used to generate Figure 2 result in maximum masses greater than  $1.442 M_\odot$ , the limit obtained from PSR 1913+16. From a theoretical perspective, it appears that values of  $R_\infty$  in the range of 12–20 km are possible for normal neutron stars whose masses are greater than  $1 M_\odot$ .

Corresponding to the two general types of EOSs, there are two general classes of neutron stars. *Normal* neutron stars are configurations with zero density at the stellar surface and which have minimum masses, of about  $0.1 M_\odot$ , that are primarily determined by the EOS below  $n_s$ . At the minimum mass, the radii are generally in excess of 100 km. The second class of stars are the so-called *self-bound* stars, which have finite density, but zero pressure, at their surfaces. They are represented in Figure 2 by strange quark matter stars (SQM1–3).

Self-bound stars have no minimum mass, unlike the case of normal neutron stars for which pure neutron matter is unbound. Unlike normal neutron stars, the maximum mass

self-bound stars have nearly the largest radii possible for a given EOS. If the strange quark mass  $m_s = 0$  and interactions are neglected ( $\alpha_c = 0$ ), the maximum mass is related to the bag constant  $B$  in the MIT-type bag model by  $M_{max} = 2.033 (56 \text{ MeV fm}^{-3}/B)^{1/2} M_\odot$ . Prakash et al. (1990) and Lattimer et al. (1990) showed that the addition of a finite strange quark mass and/or interactions produces larger maximum masses. The constraint that  $M_{max} > 1.44 M_\odot$  is thus automatically satisfied for all cases by the condition that the energy ceiling is 939 MeV. In addition, models satisfying the energy ceiling constraint, with any values of  $m_s$  and  $\alpha_c$ , have larger radii for every mass than the case SQM1. For the MIT model, the locus of maximum masses of self-bound stars is given simply by  $R \cong 1.85R_s$  (Lattimer et al. 1990), where  $R_s = 2GM/Rc^2$  is the Schwarzschild radius, which is shown in the right-hand panel of Figure 2. Strange quark stars with electrostatically supported normal-matter crusts (Glendenning & Weber 1992) have larger radii than those with bare surfaces. Coupled with the additional constraint  $M > 1M_\odot$  from protoneutron star models, MIT-model strange quark stars cannot have  $R < 8.5 \text{ km}$  or  $R_\infty < 10.5 \text{ km}$ . These values are comparable to the possible lower limits for a Bose (pion or kaon) condensate EOS.

Although the  $M - R$  trajectories for normal stars can be strikingly different, in the mass range from 1 to  $1.5 M_\odot$  or more it is usually the case that the radius has relatively little dependence upon the stellar mass. The major exceptions illustrated are the model GS1, in which a mixed phase containing a kaon condensate appears at a relatively low density and the model PAL6 which has an extremely small nuclear incompressibility (120 MeV). Both of these have considerable softening and a large increase in central density for  $M > 1 M_\odot$ . Pronounced softening, while not as dramatic, also occurs in models GS2 and PCL2, which contain mixed phases containing a kaon condensate and strange quark matter, respectively. All other normal EOSs in this figure, except PS, contain only baryons among the hadrons.

While it is generally assumed that a stiff EOS implies both a large maximum mass and a large radius, many counter examples exist. For example, GM3, MS1 and PS have relatively small maximum masses but have large radii compared to most other EOSs with larger maximum masses. Also, not all EOSs with extreme softening have small radii for  $M > 1 M_\odot$  (e.g., GS2, PS). Nonetheless, for stars with masses greater than  $1 M_\odot$ , only models with a large degree of softening (including strange quark matter configurations) can have  $R_\infty < 12$  km. Should the radius of a neutron star ever be accurately determined to satisfy  $R_\infty < 12$  km, a strong case could be made for the existence of extreme softening.

To understand the relative insensitivity of the radius to the mass for normal neutron stars, it is relevant that a Newtonian polytrope with  $n = 1$  has the property that the stellar radius is independent of both the mass and central density. Recall that most EOSs, in the density range of  $n_s - 2n_s$ , have an effective polytropic index of about one (see Figure 1). An  $n = 1$  polytrope also has the property that the radius is proportional to the square root of the constant  $K$  in the polytropic pressure law  $P = K\rho^{1+1/n}$ . This suggests that there might be a quantitative relation between the radius and the pressure that does not depend upon the EOS at the highest densities, which determines the overall softness or stiffness (and hence, the maximum mass).

In fact, this conjecture may be verified. Figure 3 shows the remarkable empirical correlation which exists between the radii of 1 and  $1.4 M_\odot$  normal stars and the matter’s pressure evaluated at fiducial densities of 1, 1.5 and  $2 n_s$ . Table 1 explains the EOS symbols used in Figure 3. Despite the relative insensitivity of radius to mass for a particular EOS in this mass range, the nominal radius  $R_M$ , which is defined as the radius at a particular mass  $M$  in solar units, still varies widely with the EOS employed. Up to  $\sim 5$  km differences are seen in  $R_{1.4}$ , for example. Of the EOSs in Table 1, the only severe violations of this correlation occurs for PCL2 and PAL6 at  $1.4 M_\odot$  for  $n_s$ , and for PS at both 1 and 1.4



$M_\odot$  for  $2n_s$ . In the case of PCL2, this is relatively close to the maximum mass, and the matter has extreme softening due to the existence of a mixed phase with quark matter. (A GS model intermediate between GS1 and GS2, with a maximum mass of  $1.44 M_\odot$ , would give similar results.) In the case of PS, it is clear from Figure 1 that extensive softening occurs already by  $1.5n_s$ . We emphasize that this correlation is valid only for cold, catalyzed neutron stars, i.e., not for protoneutron stars which have finite entropies and might contain trapped neutrinos.

Numerically, the correlation has the form of a power law:

$$R_M \simeq C(n, M) [P(n)]^{0.23-0.26}, \quad (5)$$

where  $P(n)$  is the total pressure inclusive of leptonic contributions evaluated at the density  $n$ , and  $C(n, M)$  is a number that depends on the density  $n$  at which the pressure was evaluated and the stellar mass  $M$ . An exponent of  $1/4$  was chosen for display in Figure 3, but the correlation holds for a small range of exponents about this value. Using an exponent of  $1/4$ , and ignoring points associated with EOSs with phase transitions in the density ranges of interest, we find values for  $C(n, M)$ , in units of  $\text{km fm}^{3/4} \text{ MeV}^{-1/4}$ , which are listed in Table 3. The error bars are taken from the standard deviations. The correlation is seen to be somewhat tighter for the baryon density  $n = 1.5n_s$  and  $2n_s$  cases.

The fact that the exponent is considerably less than the Newtonian value of  $1/2$  can be quantitatively understood by considering a relativistic generalization of the  $n = 1$  polytrope due to Buchdahl (1967). He found that the EOS

$$\rho = 12\sqrt{p_*P} - 5P, \quad (6)$$

where  $p_*$  is a constant fiducial pressure independent of density, has an analytic solution of Einstein's equations. This solution is characterized by the quantities  $p_*$  and  $\beta \equiv GM/Rc^2$ ,

and the stellar radius is found to be

$$R = (1 - \beta)c^2 \sqrt{\frac{\pi}{288p_*G(1 - 2\beta)}}. \quad (7)$$

For completeness, we summarize below the metric functions, the pressure and the mass-energy density as functions of coordinate radius  $r$ :

$$\begin{aligned} e^\nu &\equiv g_{tt} = (1 - 2\beta)(1 - \beta - u)(1 - \beta + u)^{-1}; \\ e^\lambda &\equiv g_{rr} = (1 - 2\beta)(1 - \beta + u)(1 - \beta - u)^{-1}(1 - \beta + \beta \cos Ar')^{-2}; \\ 8\pi PG/c^4 &= A^2 u^2 (1 - 2\beta)(1 - \beta + u)^{-2}; \\ 8\pi \rho G/c^2 &= 2A^2 u (1 - 2\beta)(1 - \beta - 3u/2)(1 - \beta + u)^{-2}. \end{aligned} \quad (8)$$

where

$$\begin{aligned} r &= r'(1 - \beta + u)(1 - 2\beta)^{-1}; \\ u &= \beta(Ar')^{-1} \sin Ar'; \\ A^2 &= 288\pi p_* G c^{-4} (1 - 2\beta)^{-1}. \end{aligned} \quad (9)$$

Note that  $R \propto p_*^{-1/2}(1 + \beta^2/2 + \dots)$ , so for a given value of  $p_*$ , the radius increases very slowly with mass.

To estimate the exponent, it is instructive to analyze the response of  $R$  to a change of pressure at some fiducial density  $\rho$ , for a fixed mass  $M$ . (At the relatively low densities of interest, the difference between using  $n$  or  $\rho$  in the following analysis is not significant.) We find the exponent to be

$$\begin{aligned} \left. \frac{d \ln R}{d \ln P} \right|_{\rho, M} &= \left. \frac{d \ln R}{d \ln p_*} \right|_{\beta} \left. \frac{d \ln p_*}{d \ln P} \right|_{\rho} \left[ 1 + \left. \frac{d \ln R}{d \ln \beta} \right|_{p_*} \right]^{-1} \\ &= \frac{1}{2} \left( 1 - \frac{5}{6} \sqrt{\frac{P}{p_*}} \right) \frac{(1 - \beta)(1 - 2\beta)}{(1 - 3\beta + 3\beta^2)}. \end{aligned} \quad (10)$$

In the limit  $\beta \rightarrow 0$ , one has  $P \rightarrow 0$  and the exponent  $d \ln R/d \ln P|_{\rho, M} \rightarrow 1/2$ , the value characteristic of an  $n = 1$  Newtonian polytrope. Finite values of  $\beta$  and  $P$  render

the exponent smaller than  $1/2$ . If the stellar mass and radius are about  $1.4 M_\odot$  and 15 km, respectively, for example, equation (7) gives  $p_* = \pi/(288R^2) \approx 4.85 \cdot 10^{-5} \text{ km}^{-2}$  (in geometrized units). Furthermore, if the fiducial density is  $\rho \approx 1.5m_b n_s \approx 2.02 \cdot 10^{-4} \text{ km}^{-2}$  (also in geometrized units, with  $m_b$  the baryon mass), equation (6) implies that in geometrized units  $P \approx 8.5 \cdot 10^{-6} \text{ km}^{-2}$ . Since the value of  $\beta$  in this case is 0.14, one then obtains  $d \ln R/d \ln P \simeq 0.31$ . This result, while mildly sensitive to the choices for  $\rho$  and  $R$ , provides a reasonable explanation of the correlation, equation (5). The fact that the exponent is smaller than  $1/2$  is clearly an effect due to general relativity.

The existence of this correlation is significant because the pressure of degenerate neutron-star matter near the nuclear saturation density  $n_s$  is, in large part, determined by the symmetry properties of the EOS, as we now discuss. Thus, the measurement of a neutron star radius, if not so small as to indicate extreme softening, could provide an important clue to the symmetry properties of matter. In either case, valuable information will be obtained.

Studies of pure neutron matter strongly suggest that the specific energy of nuclear matter near the saturation density may be expressed as an expansion quadratic in the asymmetry  $(1 - 2x)$ , where  $x$  is the proton fraction, which can be terminated after only one term (Prakash, Ainsworth & Lattimer 1988). In this case, the energy per particle and pressure of cold, beta stable nucleonic matter is

$$\begin{aligned} E(n, x) &\simeq E(n, 1/2) + S_v(n)(1 - 2x)^2, \\ P(n, x) &\simeq n^2[E'(n, 1/2) + S'_v(1 - 2x)^2], \end{aligned} \tag{11}$$

where  $E(n, 1/2)$  is the energy per particle of symmetric matter and  $S_v(n)$  is the bulk symmetry energy (which is density dependent). Primes denote derivatives with respect to density. At  $n_s$ , the symmetry energy can be estimated from nuclear mass systematics and has the value  $S_v \equiv S_v(n_s) \approx 27 - 36 \text{ MeV}$ . Attempts to further restrict this range from

consideration of fission barriers and the energies of giant resonances have led to ambiguous results. Both the magnitude of  $S_v$  and its density dependence  $S_v(n)$  are currently uncertain. Part of the symmetry energy is due to the kinetic energy for noninteracting matter, which for degenerate nucleonic matter is proportional to  $n^{2/3}$ , but the remainder of the symmetry energy, due to interactions, is also expected to contribute significantly to the overall density dependence.

Leptonic contributions must to be added to equation (11) to obtain the total energy and pressure; the electron energy per baryon is  $(3/4)\hbar cx(3\pi^2 nx)^{1/3}$ . Matter in neutron stars is in beta equilibrium, i.e.,  $\mu_e = \mu_n - \mu_p = -\partial E/\partial x$ , which permits the evaluation of the equilibrium proton fraction and the total pressure  $P$  may be written at a particular density in terms of fundamental nuclear parameters (Prakash 1996). For example, the pressure at the saturation density is simply

$$P_s = n_s(1 - 2x_s)[n_s S'_v(1 - 2x_s) + S_v x_s], \quad (12)$$

where  $S'_v \equiv (\partial S_v(n)/\partial n)_{n=n_s}$  and the equilibrium proton fraction at  $n_s$  is

$$x_s \simeq (3\pi^2 n_s)^{-1}(4S_v/\hbar c)^3 \simeq 0.04, \quad (13)$$

for  $S_v = 30$  MeV. Due to the small value of  $x_s$ , we find that  $P_s \simeq n_s S'_v$ . The inclusion of muons, which generally begin to appear around  $n_s$ , does not qualitatively affect these results.

Were we to evaluate the pressure at a larger density, contributions featuring other nuclear parameters, including the nuclear incompressibility  $K_s = 9(dP/dn)|_{n_s}$  and the skewness  $K'_s = -27n_s^3(d^3E/dn^3)|_{n_s}$ , also become significant. For analytical purposes, the nuclear matter energy per baryon, in MeV, may be expanded in the vicinity of  $n_s$  as

$$E(n, 1/2) = -16 + \frac{K_s}{18} \left(\frac{n}{n_s} - 1\right)^2 - \frac{K'_s}{27} \left(\frac{n}{n_s} - 1\right)^3. \quad (14)$$

Experimental constraints to the compression modulus  $K_s$ , most importantly from analyses of giant monopole resonances (Blaizot et al. 1995; Youngblood et al. 1999), give  $K_s \cong 220$  MeV. The skewness parameter  $K'_s$  has been estimated to lie in the range 1780–2380 MeV (Pearson 1991, Rudaz et al. 1992), but in these calculations contributions from the surface symmetry energy were neglected. For values of  $K'_s$  this large, equation (14) cannot be used beyond about  $1.5n_s$ . Evaluating the pressure for  $n = 1.5n_s$ , we find

$$P(1.5n_s) = 2.25n_s[K_s/18 - K'_s/216 + n_s(1 - 2x)^2S'_v]. \quad (15)$$

Assuming that  $S_v(n)$  is approximately proportional to the density, as it is in most relativistic field theoretical models,  $S'_v(n) \cong S_v/n_s$ . Since the  $K_s$  and  $K'_s$  terms largely cancel, the symmetry term comprises most of the total. Once again, the result that the pressure is mostly sensitive to the density dependence of the symmetry energy is found.

The sensitivity of the radius to the symmetry energy can further demonstrated by the parametrized EOS of PAL (Prakash, Ainsworth & Lattimer 1988). The symmetry energy function  $S_v(n)$  is a direct input in this parametrization and can be chosen to reproduce the results of more microscopic calculations. Figure 4 shows the dependence of mass-radius trajectories as the quantities  $S_v$  and  $S_v(n)$  are alternately varied. Clearly, of the two variations, the density dependence of  $S_v(n)$  is more important in determining the neutron star radius. Note also the weak sensitivity of the maximum neutron star mass to  $S_v$ , and that the maximum mass depends more strongly upon the function  $S_v(n)$ .

At present, experimental guidance concerning the density dependence of the symmetry energy is limited and mostly based upon the division of the nuclear symmetry energy between volume and surface contributions. Upcoming experiments involving heavy-ion collisions which might sample densities up to  $\sim (3 - 4)n_s$ , will be limited to analyzing properties of the nearly symmetric nuclear matter EOS through a study of matter, momentum, and energy flow of nucleons. Thus, studies of heavy nuclei far off the neutron

drip lines using radioactive ion beams will be necessary in order to pin down the properties of the neutron-rich regimes encountered in neutron stars.

#### 4. MOMENTS OF INERTIA

Besides the stellar radius, other global attributes of neutron stars are potentially observable, including the moment of inertia and the binding energy. These quantities depend primarily upon the ratio  $M/R$  as opposed to details of the EOS, as can be readily seen by evaluating them using analytic solutions to Einstein’s equations. Although over 100 analytic solutions to Einstein’s equations are known (Delgaty & Lake 1998), nearly all of them are physically unrealistic. However, three analytic solutions are of particular interest in normal neutron star structure.

The first is the well-known Schwarzschild interior solution for an incompressible fluid,  $\rho = \rho_c$ , where  $\rho$  is the mass-energy density. This case, hereafter referred to as “Inc”, is mostly of interest because it determines the minimum compactness  $\beta = GM/Rc^2$  for a neutron star, namely  $4/9$ , based upon the central pressure being finite. Two aspects of the incompressible fluid that are physically unrealistic, however, include the fact that the sound speed is everywhere infinite, and that the density does not vanish on the star’s surface.

The second analytic solution, due to Buchdahl (1967), is described in equation (8). We will refer to this solution as “Buch”.

The third analytic solution (which we will refer to as “T VII”) was discovered by Tolman (1939) and corresponds to the case when the mass-energy density  $\rho$  varies quadratically, that is,

$$\rho = \rho_c[1 - (r/R)^2]. \tag{16}$$

Of course, this behavior is to be expected at both extremes  $r \rightarrow 0$  and  $r \rightarrow R$ . However,

this is also an eminently reasonable representation for intermediate regions, as displayed in Figure 5, which contains results for neutron stars more massive than  $1.2 M_{\odot}$ . A wide variety of EOSs are sampled in this figure, and they are listed in Table 1.

Because the T VII solution is often overlooked in the literature (for exceptions, see, for example, Durgapal & Pande 1980 and Delgaty & Lake 1998), it is summarized here. It is useful in establishing interesting and simple relations that are insensitive to the EOS. In terms of the variable  $x = r^2/R^2$  and the compactness parameter  $\beta = GM/Rc^2$ , the assumption  $\rho = \rho_c(1 - x)$  results in  $\rho_c = 15\beta c^2/(8\pi GR^2)$ . The solution of Einstein’s equations for this density distribution is:

$$\begin{aligned} e^{-\lambda} &= 1 - \beta x(5 - 3x), & e^{\nu} &= (1 - 5\beta/3) \cos^2 \phi, \\ P &= \frac{c^4}{4\pi R^2 G} \left[ \sqrt{3\beta e^{-\lambda}} \tan \phi - \frac{\beta}{2}(5 - 3x) \right], & n &= \frac{(\rho c^2 + P) \cos \phi}{m_b c^2 \cos \phi_1}, \\ \phi &= (w_1 - w)/2 + \phi_1, & w &= \log \left[ x - 5/6 + \sqrt{e^{-\lambda}/(3\beta)} \right], \\ \phi_c &= \phi(x = 0), & \phi_1 &= \phi(x = 1) = \tan^{-1} \sqrt{\beta/[3(1 - 2\beta)]}, & w_1 &= w(x = 1). \end{aligned} \quad (17)$$

The central values of  $P/\rho c^2$  and the square of the sound speed  $c_s^2$  are

$$\left. \frac{P}{\rho c^2} \right|_c = \frac{2}{15} \sqrt{\frac{3}{\beta}} \left( \frac{c_s}{c} \right)^2, \quad \left( \frac{c_s}{c} \right)^2 = \tan \phi_c \left( \tan \phi_c + \sqrt{\frac{\beta}{3}} \right). \quad (18)$$

This solution, like that of Buchdahl’s, is scale-free, with the parameters  $\beta$  and  $\rho_c$  (or  $M$  and  $R$ ). There are obvious limitations to the range of parameters for realistic models: when  $\phi_c = \pi/2$ , or  $\beta \approx 0.3862$ ,  $P_c$  becomes infinite, and when  $\beta \approx 0.2698$ ,  $c_s$  becomes causal (i.e.,  $c$ ). Recall that for an incompressible fluid,  $P_c$  becomes infinite when  $\beta = 4/9$ , and this EOS is acausal for all values of  $\beta$ . For the Buchdahl solution,  $P_c$  becomes infinite when  $\beta = 2/5$  and the causal limit is reached when  $\beta = 1/6$ . For comparison, the causal limit for realistic EOSs is  $\beta \cong 0.33$  (Lattimer et al. 1990, Glendenning 1992), as previously discussed.

The general applicability of these exact solutions can be gauged by analyzing the

moment of inertia, which, for a star uniformly rotating with angular velocity  $\Omega$ , is

$$I = (8\pi/3) \int_0^R r^4 (\rho + P/c^2) e^{(\lambda-\nu)/2} (\omega/\Omega) dr. \quad (19)$$

The metric function  $\omega$  is a solution of the equation

$$d[r^4 e^{-(\lambda+\nu)/2} \omega']/dr + 4r^3 \omega de^{-(\lambda+\nu)/2}/dr = 0 \quad (20)$$

with the surface boundary condition

$$\omega_R = \Omega - \frac{R}{3} \omega'_R = \Omega \left[ 1 - \frac{2GI}{R^3 c^2} \right]. \quad (21)$$

The second equality in the above follows from the definition of  $I$  and the TOV equation.

Writing  $j = \exp[-(\nu + \lambda)/2]$ , the TOV equation becomes

$$j' = -4\pi G r (P/c^2 + \rho) j e^{\lambda/c^2}. \quad (22)$$

Then, one has

$$I = -\frac{2c^2}{3G} \int \frac{\omega}{\Omega} r^3 dj = \frac{c^2 R^4 \omega'_R}{6G\Omega}. \quad (23)$$

Unfortunately, an analytic representation of  $\omega$  or the moment of inertia for any of the three exact solutions is not available. However, approximations which are valid in the causal regime to within 0.5% are

$$I_{Inc}/MR^2 \simeq 2(1 - 0.87\beta - 0.3\beta^2)^{-1}/5, \quad (24)$$

$$I_{Buch}/MR^2 \simeq (2/3 - 4/\pi^2)(1 - 1.81\beta + 0.47\beta^2)^{-1}, \quad (25)$$

$$I_{TVII}/MR^2 \simeq 2(1 - 1.1\beta - 0.6\beta^2)^{-1}/7. \quad (26)$$

In each case, the small  $\beta$  limit gives the corresponding Newtonian result. Figure 6 indicates that the T VII approximation is a rather good approximation to most EOSs without extreme softening at high densities, for  $M/R \geq 0.1 M_\odot/\text{km}$ . The EOSs with softening fall below this trajectory. Ravenhall & Pethick (1994) had suggested the expression

$$I_{RP}/MR^2 \simeq 0.21/(1 - 2\beta) \quad (27)$$



as an approximation for the moment of inertia; however, we find that this expression is not a good overall fit, as shown in Figure 6.

For low-mass stars, none of the analytic approximations are suitable, and the moment of inertia deviates substantially from the behavior of an incompressible fluid. Although neutron stars of such small mass are unlikely to exist, it is interesting to examine the behavior of  $I$  in the limit of small compactness, especially the surprising result that  $I/MR^2 \rightarrow 0$  as  $\beta \rightarrow 0$ . It is well known from the work of Baym, Bethe & Pethick (1971) that the adiabatic index of matter below nuclear density is near to, but less than  $4/3$ . As the compactness parameter  $\beta$  decreases, a greater fraction of the star’s mass lies below  $n_s$ . To the extent that these stars can be approximated as polytropes (i.e., having a constant polytropic index  $n$ ), Table 4 shows how the quantity  $I/MR^2$  varies with  $n$ . For a polytropic index of 3, corresponding to an adiabatic exponent of  $4/3$ ,  $I/MR^2 \simeq 0.075$ , considerably lower than the value of 0.4 for an incompressible fluid. Calculations of matter at subnuclear density agree on the fact that the adiabatic exponent of matter further decreases with decreasing density, until the neutron drip point (near  $4.3 \times 10^{11}$  g cm $^{-3}$ ) is approached and the exponent is near zero. Although the central densities of minimum mass neutron stars are about  $2 \times 10^{14}$  g cm $^{-3}$ , much of the mass of the star is at considerably lower density, unlike the situation for solar mass-sized neutron stars which are relatively centrally condensed. Thus, as  $\beta$  decreases, the quantity  $I/MR^2$  rapidly decreases, approaching the limiting value of zero as an effective polytropic index of nearly 5 is achieved.

Another interesting result from Figure 6 concerns the moments of inertia of strange quark matter stars. Such stars are relatively closely approximated by incompressible fluids, this behavior becoming exact in the limit of  $\beta \rightarrow 0$ . This could have been anticipated from the  $M \propto R^3$  behavior of the  $M - R$  trajectories for small  $\beta$  strange quark matter stars as observed in Figure 2.

## 5. CRUSTAL FRACTION OF THE MOMENT OF INERTIA

A new observational constraint involving  $I$  concerns pulsar glitches. Occasionally, the spin rate of a pulsar will suddenly increase (by about a part in  $10^6$ ) without warning after years of almost perfectly predictable behavior. However, Link, Epstein & Lattimer (1999) argue that these glitches are not completely random: the Vela pulsar experiences a sudden spinup about every three years, before returning to its normal rate of slowing. Also, the size of a glitch seems correlated with the interval since the previous glitch, indicating that they represent self-regulating instabilities for which the star prepares over a waiting time. The angular momentum requirements of glitches in Vela imply that  $\geq 1.4\%$  of the star’s moment of inertia drives these events.

Glitches are thought to represent angular momentum transfer between the crust and another component of the star. In this picture, as a neutron star’s crust spins down under magnetic torque, differential rotation develops between the stellar crust and this component. The more rapidly rotating component then acts as an angular momentum reservoir which occasionally exerts a spin-up torque on the crust as a consequence of an instability. A popular notion at present is that the freely spinning component is a superfluid flowing through a rigid matrix in the thin crust, the region in which dripped neutrons coexist with nuclei, of the star. As the solid portion is slowed by electromagnetic forces, the liquid continues to rotate at a constant speed, just as superfluid He continues to spin long after its container has stopped. This superfluid is usually assumed to locate in the star’s crust, which thus must contain at least 1.4% of the star’s moment of inertia.

The high-density boundary of the crust is naturally set by the phase boundary between nuclei and uniform matter, where the pressure is  $P_t$  and the density  $n_t$ . The low-density boundary is the neutron drip density, or for all practical purposes, simply the star’s surface since the amount of mass between the neutron drip point and the surface is negligible. One

can utilize equation (19) to determine the moment of inertia of the crust along with the assumptions that  $P/c^2 \ll \rho$ ,  $m(r) \simeq M$ , and  $\omega_j \simeq \omega_R$  in the crust. Defining  $\Delta R$  to be the crust thickness, that is, the distance between the surface and the point where  $P = P_t$ ,

$$\Delta I \simeq \frac{8\pi}{3} \frac{\omega_R}{\Omega} \int_{R-\Delta R}^R \rho r^4 e^\lambda dr \simeq \frac{8\pi}{3GM} \frac{\omega_R}{\Omega} \int_0^{P_t} r^6 dP, \quad (28)$$

where  $M$  is the star's total mass and the TOV equation was used in the last step. In the crust, the fact that the EOS is of the approximate polytropic form  $P \simeq K\rho^{4/3}$  can be used to find an approximation for the integral  $\int r^6 dP$ , *viz.*

$$\int_0^{P_t} r^6 dP \simeq P_t R^6 \left[ 1 + \frac{2P_t}{n_t m_n c^2} \frac{(1+7\beta)(1-2\beta)}{\beta^2} \right]^{-1}. \quad (29)$$

For most neutron stars, the approximation equation (26) gives  $I$  in terms of  $M$  and  $R$ , and equation (21) gives  $\omega_R/\Omega$  in terms of  $I$  and  $R$ , the quantity  $\Delta I/I$  can thus be cast as a function of  $M$  and  $R$  with the only dependences upon the EOS arising from the values of  $P_t$  and  $n_t$ ; there is no explicit dependence upon the EOS at any other density. However, the major dependence is mostly upon the value of  $P_t$ , since  $n_t$  enters only as a correction. We then find

$$\frac{\Delta I}{I} \simeq \frac{28\pi P_t R^3 (1 - 1.67\beta - 0.6\beta^2)}{3Mc^2 \beta} \left[ 1 + \frac{2P_t(1 + 5\beta - 14\beta^2)}{n_t m_b c^2 \beta^2} \right]^{-1}. \quad (30)$$

In general, the EOS parameter  $P_t$ , in the units of  $\text{MeV fm}^{-3}$ , varies over the range  $0.25 < P_t < 0.65$  for realistic EOSs. The determination of this parameter requires a calculation of the structure of matter containing nuclei just below nuclear matter density that is consistent with the assumed nuclear matter EOS. Unfortunately, few such calculations have been performed. Like the fiducial pressure at and above nuclear density which appears in equation (5),  $P_t$  should depend sensitively upon the behavior of the symmetry energy near nuclear density.

Since the calculation of the pressure below nuclear density has not been consistently done for most realistic EOSs, we arbitrarily choose  $n_t = 0.07 \text{ fm}^{-3}$  and compare the

approximation equation (30) with the results of full structural calculations in Figure 7. Two extreme values of  $P_t$  were assumed in the full structural calculations to identify the core-crust boundary. Irrespective of this choice, the agreement between the analytical estimate equation (30) and the full calculations appears to be good for all EOSs, including ones with extreme softening. We also note that Ravenhall & Pethick (1994) developed a different, but nearly equivalent, analytic formula for the quantity  $\Delta I/I$  as a function of  $M, R, P_t$  and  $\mu_t$ , where  $\mu_t$  is the neutron chemical potential at the core-crust phase boundary. This prediction is also displayed in Figure 7.

Link, Epstein & Lattimer (1999) established a lower limit to the radius of the Vela pulsar by using equation (30) with  $P_t$  at its maximum value and the glitch constraint  $\Delta I/I \geq 0.014$ . A minimum radius can be found by combining this constraint with the largest realistic value of  $P_t$  from any equation of state, namely about  $0.65 \text{ MeV fm}^{-3}$ . Stellar models that are compatible with this constraint must fall to the right of the  $P_t = 0.65 \text{ MeV fm}^{-3}$  contour in Figure 7. This imposes a constraint upon the radius, which is approximately equivalent to

$$R > 3.9 + 3.5M/M_\odot - 0.08(M/M_\odot)^2 \text{ km} . \quad (31)$$

As shown in the figure, this constraint is somewhat more stringent than one based upon causality. Better estimates of the maximum value of  $P_t$  should make this constraint more stringent.

## 6. BINDING ENERGIES

The binding energy formally represents the energy gained by assembling  $N$  baryons. If the baryon mass is  $m_b$ , the binding energy is simply  $BE = Nm_b - M$  in mass units. However, the quantity  $m_b$  has various interpretations in the literature. Some authors take

it to be  $939 \text{ MeV}/c^2$ , the same as the neutron or proton mass. Others take it to be about  $930 \text{ MeV}/c^2$ , corresponding to the mass of  $\text{C}^{12}/12$  or  $\text{Fe}^{56}/56$ . The latter choice would be more appropriate if  $BE$  was to represent the energy released in by the collapse of a white-dwarf-like iron core in a supernova explosion. The difference in these definitions,  $10 \text{ MeV}$  per baryon, corresponds to a shift of  $10/939 \simeq 0.01$  in the value of  $BE/M$ . This energy,  $BE$ , can be deduced from neutrinos detected from a supernova event; indeed, it might be the most precisely determined aspect of the neutrino signal.

Lattimer & Yahil (1989) suggested that the binding energy could be approximated as

$$BE \approx 1.5 \cdot 10^{51} (M/M_{\odot})^2 \text{ ergs} = 0.084 (M/M_{\odot})^2 M_{\odot}. \quad (32)$$

Prakash et al. (1997) also concluded that such a formula was a reasonable approximation, based upon a comparison of selected non-relativistic potential and field-theoretical models. In Figure 8, this formula is compared to exact results, which shows that it is accurate at best to about  $\pm 20\%$ . The largest deviations are for stars with extreme softening or large mass.

Here, we propose a more accurate representation of the binding energy:

$$BE/M \simeq 0.6\beta/(1 - 0.5\beta), \quad (33)$$

which incorporates some radius dependence. Thus, the observation of supernova neutrinos, and the estimate of the total radiated neutrino energy, will yield more accurate information about  $M/R$  than about  $M$  alone.

In the cases of the incompressible fluid and the Buchdahl solution, analytic results for the binding energy can be found:

$$BE_{Inc}/M = \frac{3}{4\beta} \left( \frac{\sin^{-1} \sqrt{2\beta}}{\sqrt{2\beta}} - \sqrt{1 - 2\beta} \right) - 1 \approx \frac{3\beta}{5} + \frac{9\beta^2}{14} + \frac{5\beta^3}{6} + \dots; \quad (34)$$

$$BE_{Buch}/M = (1 - 1.5\beta)(1 - 2\beta)^{-1/2}(1 - \beta)^{-1} - 1 \approx \frac{\beta}{2} + \frac{\beta^2}{2} + \frac{3\beta^3}{4} + \dots. \quad (35)$$

In addition, an expansion for the T VII solution can be found:

$$BE_{TVII}/M \approx \frac{11\beta}{21} + \frac{7187\beta^2}{18018} + \frac{68371\beta^3}{306306} + \dots . \quad (36)$$

The exact results for the three analytic solutions of Einstein’s equations, as well as the fit of equation (33), are compared to some EOSs in Figure 9. It can be seen that for stars without extreme softening both the T VII and Buch solutions are rather realistic. However, for EOSs with softening, the deviations from this can be substantial. Thus, until information about the existence of softening in neutron stars is available, the binding energy alone provides only limited information about the star’s structure or mass.

## 7. SUMMARY AND OUTLOOK

We have demonstrated the existence of a strong correlation between the pressure near nuclear saturation density inside a neutron star and the radius which is relatively insensitive to the neutron star’s mass and equation of state for normal neutron stars. In turn, the pressure near the saturation density is primarily determined by the isospin properties of the nucleon-nucleon interaction, specifically, as reflected in the density dependence of the symmetry energy,  $S_v(n)$ . This result is not sensitive to the other nuclear parameters such as  $K_s$ , the nuclear incompressibility parameter, or  $K'_s$ , the skewness parameter. This is important, because the value of the symmetry energy at nuclear saturation density and the density dependence of the symmetry energy are both difficult to determine in the laboratory. Thus, a measurement of a neutron star’s radius would yield important information about these quantities.

Any measurement of a radius will have some intrinsic uncertainty. In addition, the empirical relation we have determined between the pressure and radius has a small uncertainty. It is useful to display how accurately the equation of state might be established

from an eventual radius measurement. This can be done by inverting equation (5), which yields

$$P(n) \simeq [R_M/C(n, M)]^4. \quad (37)$$

The inferred ranges of pressures, as a function of density and for three possible values of  $R_{1.4}$ , are shown in Figure 10. It is assumed that the mass is  $1.4 M_\odot$ , but the results are relatively insensitive to the actual mass. Note from Table 3 that the differences between  $C$  for 1 and  $1.4 M_\odot$  are typically less than the errors in  $C$  itself. The light shaded areas show the pressures including only errors associated with  $C$ . The dark shaded areas show the pressures when a hypothetical observational error of 0.5 km is also taken into account. These results suggest that a useful restriction to the equation of state is possible if the radius of a neutron star can be measured to an accuracy better than about 1 km.

The reason useful constraints might be obtained from just a single measurement of a neutron star radius, rather than requiring a series of simultaneous mass-radii measurements as Lindblom (1992) proposed, stems from the fact that we have been able to establish the empirical correlation, equation (5). In turn, it appears that this correlation exists because most equations of state have slopes  $d \ln P / d \ln n \simeq 2$  near  $n_s$ .

The best prospect for measuring a neutron star’s radius may be the nearby object RX J185635-3754. It is anticipated that parallax information for this object will be soon available (Walter, private communication). In addition, it may be possible to identify spectral lines with the Chandra and XMM X-ray facilities that would not only yield the gravitational redshift, but would identify the atmospheric composition. Not only would this additional information reduce the uncertainty in value of  $R_\infty$ , but, *both* the mass and radius for this object might thereby be determined. It is also possible that an estimate of the surface gravity of the star can be found from further comparisons of observations with atmospheric modelling, and this would provide a further check on the mass and radius.

We have presented simple expressions for the moment of inertia, the binding energy, and the crustal fraction of the moment of inertia for normal neutron stars which are largely independent of the EOS. If the magnitudes of observed glitches from Vela are connected with the crustal fraction of moment of inertia, the formula we derived establishes a more stringent limit on the radius than causality.

We thank A. Akmal, V. R. Pandharipande and J. Schaffner-Bielich for making the results of their equation of state calculations available to us in tabular form. This work was supported in part by the USDOE grants DOE/DE-FG02-87ER-40317 & DOE/DE-FG02-88ER-40388.

## REFERENCES

- Akmal, A. & Pandharipande, V.R. 1997, *Phys. Rev.*, C56, 2261
- Alcock, C. & Olinto, A. 1988, *Ann. Rev. Nucl. Sci.*, 38, 161
- Alpar, A. & Shaham, J. 1985, *Nature*, 316, 239
- An, P., Lattimer, J.M., Prakash, M. & Walter, F. 2000, in preparation
- Baym, G., Pethick, C. J. & Sutherland, P. 1971, *ApJ*, 170, 299
- Blaizot, J.P., Berger, J.F., Dechargé, J. & Girod, M. 1995, *Nucl. Phys.*, A591, 431
- Brown, G. E., Weingartner, J. C. & Wijers, R. A. M. J. 1996, *ApJ*, 463, 297
- Buchdahl, H.A. 1967, *ApJ*, 147, 310
- Delgaty, M.S.R. & Lake, K. 1998, *Computer Physics Communications*, 115, 395
- Durgapal, M.C. & Pande, A.K. 1980, *J. Pure & Applied Phys.*, 18, 171
- Engvik, L., Hjorth-Jensen, M., Osnes, E., Bao, G. & Østgaard, E. 1994, *Phys. Rev. Lett.*, 73, 2650
- 1996, *ApJ*, 469, 794
- Fahri, E. & Jaffe, R. 1984, *Phys. Rev.*, D30, 2379



- Friedman, B. & Pandharipande, V.R. 1981, Nucl. Phys., A361, 502
- Glendenning, N.K. 1992, Phys. Rev., D46, 1274
- Glendenning, N.K. & Moszkowski, S.A. 1991, Phys. Rev. Lett., 67, 2414
- Glendenning, N.K. & Schaffner-Bielich, J. 1999, Phys. Rev., C60, 025803
- Glendenning, N.K. & Weber, F. 1992, ApJ, 400, 672
- Golden, A. & Shearer, A. 1999, A&A, 342, L5
- Goussard J.-O., Haensel, P. & Zdunik, J. L. 1998, A&A, 330, 1005.
- Haensel, P., Zdunik, J. L. & Schaeffer, R. 1986, A&A, 217, 137
- Heap, S. R. & Corcoran, M. F. 1992, ApJ, 387, 340
- Inoue, H. 1992, in The Structure and Evolution of Neutron Stars, ed. D. Pines,  
R. Tamagaki and S. Tsuruta, (Redwood City: Addison Wesley, 1992) 63
- Lattimer, J.M., Pethick, C.J., Ravenhall, D.G. & Lamb, D.Q. 1985, Nucl. Phys., A432,  
646
- Lattimer, J.M., Prakash, M., Masak, D. & Yahil, A. 1990, ApJ, 355, 241
- Lattimer, J.M. & Swesty, F.D. 1991, Nucl. Phys., A535, 331
- Lattimer, J.M. & Yahil, A. 1989, ApJ, 340, 426
- Link, B., Epstein, R.I. & Lattimer, J.M. 1999, Phys. Rev. Lett., 83, 3362
- Lindblom, L. 1992, ApJ, 398, 569
- Müller, H. & Serot, B.D. 1996, Nucl. Phys., A606, 508
- Müther, H., Prakash, M. & Ainsworth, T.L. 1987, Phys. Lett., B199, 469
- Negele, J. W. & Vautherin, D. 1974, Nucl. Phys., A207, 298
- Orosz, J. A. & Kuulkers, E. 1999, MNRAS, 305, 132
- Osherovich, V. & Titarchuk, L. 1999, ApJ, 522, L113
- Page, D. 1995, ApJ, 442, 273
- Pavlov, G.G., Zavlin, V.E., Truemper, J. & Neuhauser, R. 1996, ApJ, 472, L33
- Pandharipande, V. R. & Smith, R. A. 1975, Nucl. Phys., A237, 507

- Pearson, J.M. 1991, *Phys. Lett.*, B271, 12
- Prakash, M. 1996, in *Nuclear Equation of State*, ed. A. Ansari & L. Satpathy (Singapore: World Scientific), p. 229
- Prakash, M., Ainsworth, T.L. & Lattimer, J.M. 1988, *Phys. Rev. Lett.*, 61, 2518
- Prakash, Manju., Baron, E. & Prakash, M. 1990, *Phys. Lett.*, B243, 175
- Prakash, M., Bombaci, I, Prakash, Manju., Lattimer, J.M., Ellis, P.J. & Knorren, R. 1997, *Phys. Rep.*, 280, 1
- Prakash, M., Cooke, J.R. & Lattimer, J.M. 1995, *Phys. Rev.*, D52, 661
- Psaltis, D. et al. 1998, *ApJ*, 501, L95
- Rajagopal, M., Romani, R.W. & Miller, M. C. 1997, *ApJ*, 479, 347
- Ravenhall, D.G. & Pethick, C.J. 1994, *ApJ*, 424, 846
- Rhoades, C. E. & Ruffini, R. 1974, *Phys. Rev. Lett.*, 32, 324
- Romani, R.W. 1987, *ApJ*, 313, 718
- Rudaz, S., Ellis, P. J., Heide, E. K. and Prakash, M. 1992, *Phys. Lett.*, B285, 183
- Rutledge, R., Bildstein, L., Brown, E., Pavlov, G. G. & Zavlin, V. E. AAS Meeting #193, Abstract #112.03
- Schulz, N. S. 1999, *ApJ*, 511, 304
- Stella, L. & Vietri, M. 1999, *Phys. Rev. Lett.*, 82, 17
- Stella, L., Vietri, M. & Morsink, S. 1999, *ApJ*, 524, L63
- Stickland, D. Lloyd, C. & Radzuin-Woodham, A. 1997, *MNRAS*, 286, L21
- Thorsett, S.E. & Chakrabarty, D. 1999, *ApJ*, 512, 288
- Titarchuk, L. 1994, *ApJ*, 429, 340
- Tolman, R.C. 1939, *Phys. Rev.*, 55, 364
- van Kerkwijk, J. H., van Paradijs, J. & Zuiderwijk, E. J. 1995, *A&A*, 303, 497
- Walter, F., Wolk, S. & Neuhaüser, R. 1996, *Nature*, 379, 233
- Walter, F. & Matthews, L. D. 1997, *Nature*, 389, 358

Wiringa, R.B., Fiks, V. & Fabrocine, A. 1988, Phys. Rev., C38. 1010

Witten, E. 1984, Phys. Rev., D30, 272

Youngblood, D.H., Clark, H.L. & Lui, Y.-W. 1999, Phys. Rev. Lett., 82, 691

TABLE 1

EQUATIONS OF STATE

Symbol	Reference	Approach	Composition
FP	Friedman & Pandharipande (1981)	Variational	np
PS	Pandharipande & Smith (1975)	Potential	$n\pi^0$
WFF(1-3)	Wiringa, Fiks & Fabrocine (1988)	Variational	np
AP(1-4)	Akmal & Pandharipande (1998)	Variational	np
MS(1-3)	Müller & Serot (1996)	Field Theoretical	np
MPA(1-2)	Müther, Prakash & Ainsworth (1987)	Dirac-Brueckner HF	np
ENG	Engvik et al. (1996)	Dirac-Brueckner HF	np
PAL(1-6)	Prakash, Ainsworth & Lattimer (1988)	Schematic Potential	np
GM(1-3)	Glendenning & Moszkowski (1991)	Field Theoretical	npH
GS(1-2)	Glendenning & Schaffner-Bielich (1999)	Field Theoretical	npK
PCL(1-2)	Prakash, Cooke & Lattimer (1995)	Field Theoretical	npHQ
SQM(1-3)	Prakash, Cooke & Lattimer (1995)	Quark Matter	Q ( $u, d, s$ )

NOTES.— Approach refers to the underlying theoretical technique. Composition refers to strongly interacting components (n=neutron, p=proton, H=hyperon, K=kaon, Q=quark); all models include leptonic contributions.

TABLE 2

PARAMETERS FOR SELF-BOUND STRANGE QUARK STARS

Model	$B$ (MeV fm <sup>-3</sup> )	$m_s$ (MeV)	$\alpha_c$
SQM1	94.92	0	0
SQM2	64.21	150	0.3
SQM3	57.39	50	0.6

NOTES.— Numerical values employed in the MIT bag model as described in Fahri & Jaffe (1984).

TABLE 3

THE QUANTITY  $C(n, M)$  OF EQUATION 5

$n$	1 M <sub>⊙</sub>	1.4 M <sub>⊙</sub>
$n_s$	9.53 ± 0.32	9.30 ± 0.60
1.5 $n_s$	7.14 ± 0.15	7.00 ± 0.31
2 $n_s$	5.82 ± 0.21	5.72 ± 0.25

NOTES.— The quantity  $C(n, M)$ , in units of km fm<sup>3/4</sup> MeV<sup>-1/4</sup>, which relates the pressure (evaluated at density  $n$ ) to the radius of neutron stars of mass  $M$ . The errors are standard deviations.

TABLE 4

MOMENTS OF INERTIA FOR POLYTROPES

Index $n$	$I/MR^2$	Index $n$	$I/MR^2$
0	0.4	3.5	0.045548
0.5	0.32593	4.0	0.022573
1.0	0.26138	4.5	0.0068949
1.5	0.20460	4.8	0.0014536
2.0	0.15485	4.85	0.00089178
2.5	0.11180	4.9	0.0004536
3.0	0.075356	5.0	0

NOTES.— The quantity  $I/MR^2$  for polytropes, which satisfy the relation  $P = K\rho^{1+1/n}$  ( $\rho$  is the mass-energy density), as a function of the polytropic index  $n$ .

**FIGURE CAPTIONS**

FIG. 1.—The pressure-density relation for a selected set of EOSs contained in Table 1. The pressure is in units of MeV fm<sup>-3</sup> and the density is in units of baryons per cubic fermi. The nuclear saturation density is approximately 0.16 fm<sup>-3</sup>.

FIG. 2.—Mass-radius curves for several EOSs listed in Table 1. The left panel is for stars containing nucleons and, in some cases, hyperons. The right panel is for stars containing more exotic components, such as mixed phases with kaon condensates or strange quark matter, or pure strange quark matter stars. In both panels, the lower limit causality places on  $R$  is shown as a dashed line, a constraint derived from glitches in the Vela pulsar is shown as the solid line labelled  $\Delta I/I = 0.014$ , and contours of constant  $R_\infty = R/\sqrt{1 - 2GM/Rc^2}$ , are shown as dotted curves. In the right panel, the theoretical trajectory of maximum masses and radii for pure strange quark matter stars is marked by the dot-dash curve labelled  $R = 1.85R_s$ .

FIG. 3.— Empirical relation between pressure, in units of MeV fm<sup>-3</sup>, and radius, in km, for EOSs listed in Table 1. The upper panel shows results for 1 M<sub>⊙</sub> (gravitational mass) stars; the lower panel is for 1.4 M<sub>⊙</sub> stars. The different symbols show values of  $RP^{-1/4}$  evaluated at three fiducial densities.

FIG. 4.— Left panel: Mass-radius curves for selected PAL (Prakash, Ainsworth & Lattimer 1988) forces showing the sensitivity to symmetry energy. The left panel shows variations arising from different choices of  $S_v$ , the symmetry energy evaluated at  $n_s$ ; the right panel shows variations arising from different choices of  $S_v(n)$ , the density dependent symmetry

energy. In this figure, the shorthand  $u = n/n_s$  is used.

FIG. 5.— Profiles of mass-energy density ( $\rho$ ), relative to central values ( $\rho_c$ ), in neutron stars for several EOSs listed in Table 1. For reference, the thick black lines show the simple quadratic approximation  $1 - (r/R)^2$ .

FIG. 6.— The moment of inertia  $I$ , in units of  $MR^2$ , for several EOSs listed in Table 1. The curves labelled “Inc”, “T VII”, “Buch” and “RP” are for an incompressible fluid, the Tolman (1939) VII solution, the Buchdahl (1967) solution, and an approximation of Ravenhall & Pethick (1994), respectively. The inset shows details of  $I/MR^2$  for  $M/R \rightarrow 0$ .

FIG. 7.— Mass-radius curves for selected EOSs from Table 1, comparing theoretical contours of  $\Delta I/I = 0.014$  from approximations developed in this paper, labelled “LP”, and from Ravenhall & Pethick (1994), labelled “RP”, to numerical results (solid dots). Two values of  $P_t$ , the transition pressure demarking the crust’s inner boundary, which bracket estimates in the literature, are employed. The region to the left of the  $P_t = 0.65$  MeV  $\text{fm}^{-3}$  curve is forbidden if Vela glitches are due to angular momentum transfers between the crust and core, as discussed in Link, Epstein & Lattimer (1999). For comparison, the region excluded by causality alone lies to the left of the dashed curve labelled “causality” as determined by Lattimer et al. (1990) and Glendenning (1992).

FIG. 8.— The binding energy of neutron stars as a function of stellar gravitational mass for several EOSs listed in Table 1. The predictions of equation (32), due to Lattimer & Yahil (1989), are shown by the line labelled “LY” and the shaded region.

FIG. 9.— The binding energy per unit gravitational mass as a function of compactness for



the EOSs listed in Table 1. Solid lines labelled “Inc”, “Buch” and “T VII” show predictions for an incompressible fluid, the solution of Buchdahl (1967), and the Tolman (1939) VII solution, respectively. The shaded region shows the prediction of equation (33).

FIG. 10.—The pressures inferred from the empirical correlation equation (5), for three hypothetical radius values (10, 12.5 and 15 km) overlaid on the pressure-density relations shown in Figure 1. The light shaded region takes into account only the uncertainty associated with  $C(n, M)$ ; the dark shaded region also includes a hypothetical uncertainty of 0.5 km in the radius measurement. The neutron star mass was assumed to be  $1.4 M_{\odot}$ .

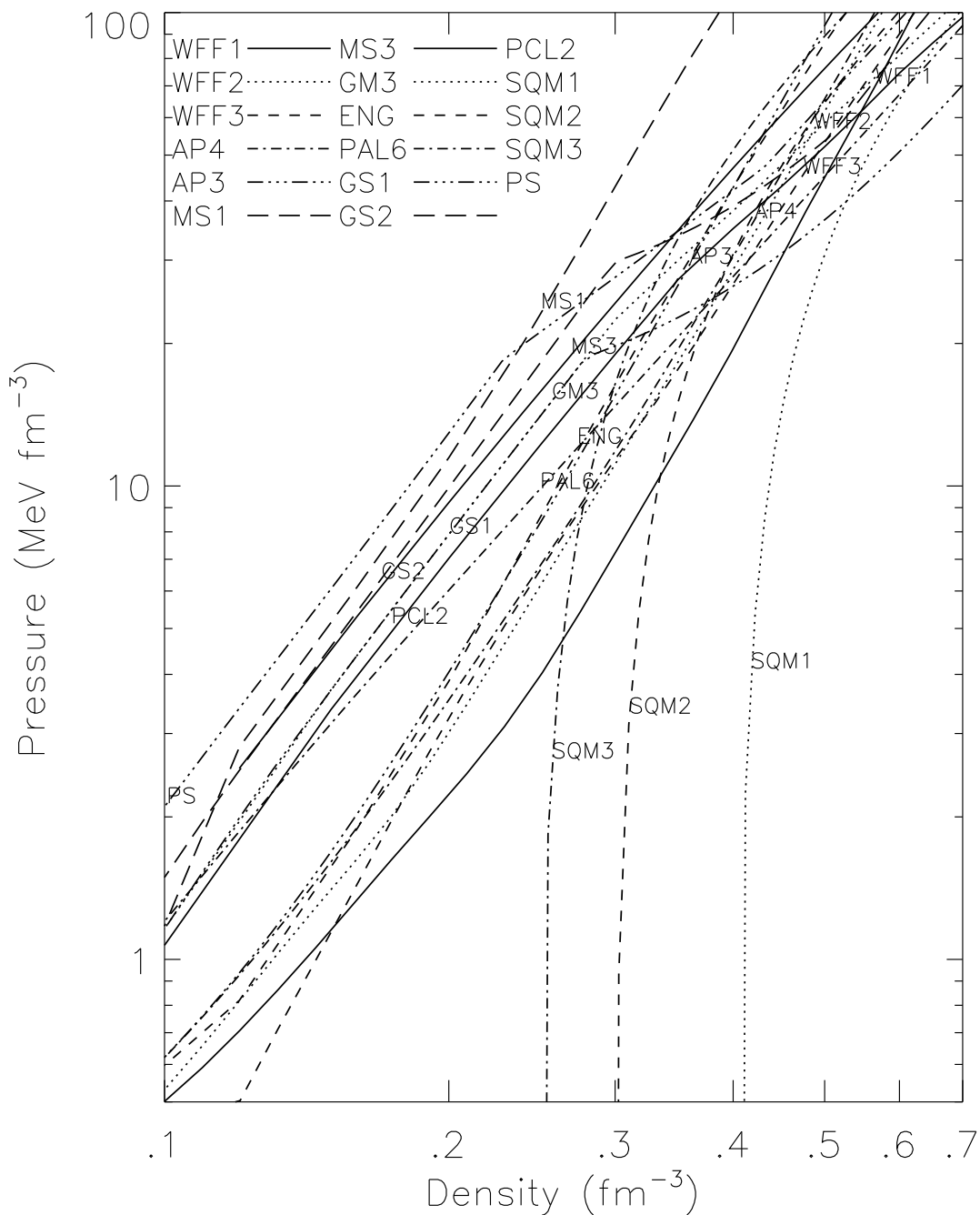


Fig. 1.— The pressure-density relation for a selected set of EOSs contained in Table 1. The pressure is in units of MeV fm<sup>-3</sup> and the density is in units of baryons per cubic fermi. The nuclear saturation density is approximately 0.16 fm<sup>-3</sup>.

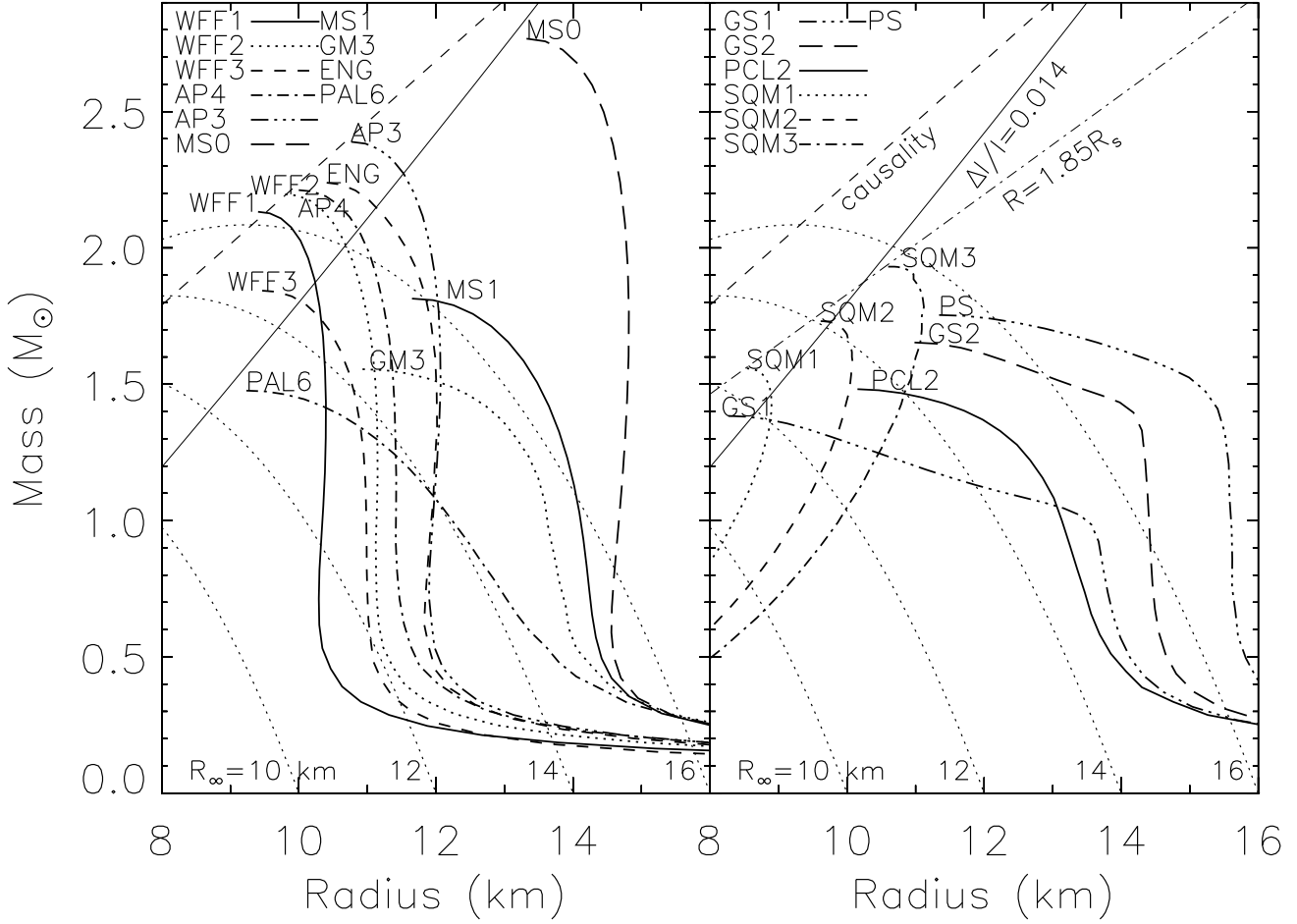


Fig. 2.— Mass-radius curves for several EOSs listed in Table 1. The left panel is for stars containing nucleons and, in some cases, hyperons. The right panel is for stars containing more exotic components, such as mixed phases with kaon condensates or strange quark matter, or pure strange quark matter stars. In both panels, the lower limit causality places on  $R$  is shown as a dashed line, a constraint derived from glitches in the Vela pulsar is shown as the solid line labelled  $\Delta I/I = 0.014$ , and contours of constant  $R_\infty = R/\sqrt{1 - 2GM/Rc^2}$  are shown as dotted curves. In the right panel, the theoretical trajectory of maximum masses and radii for pure strange quark matter stars is marked by the dot-dash curve labelled  $R = 1.85R_s$ .

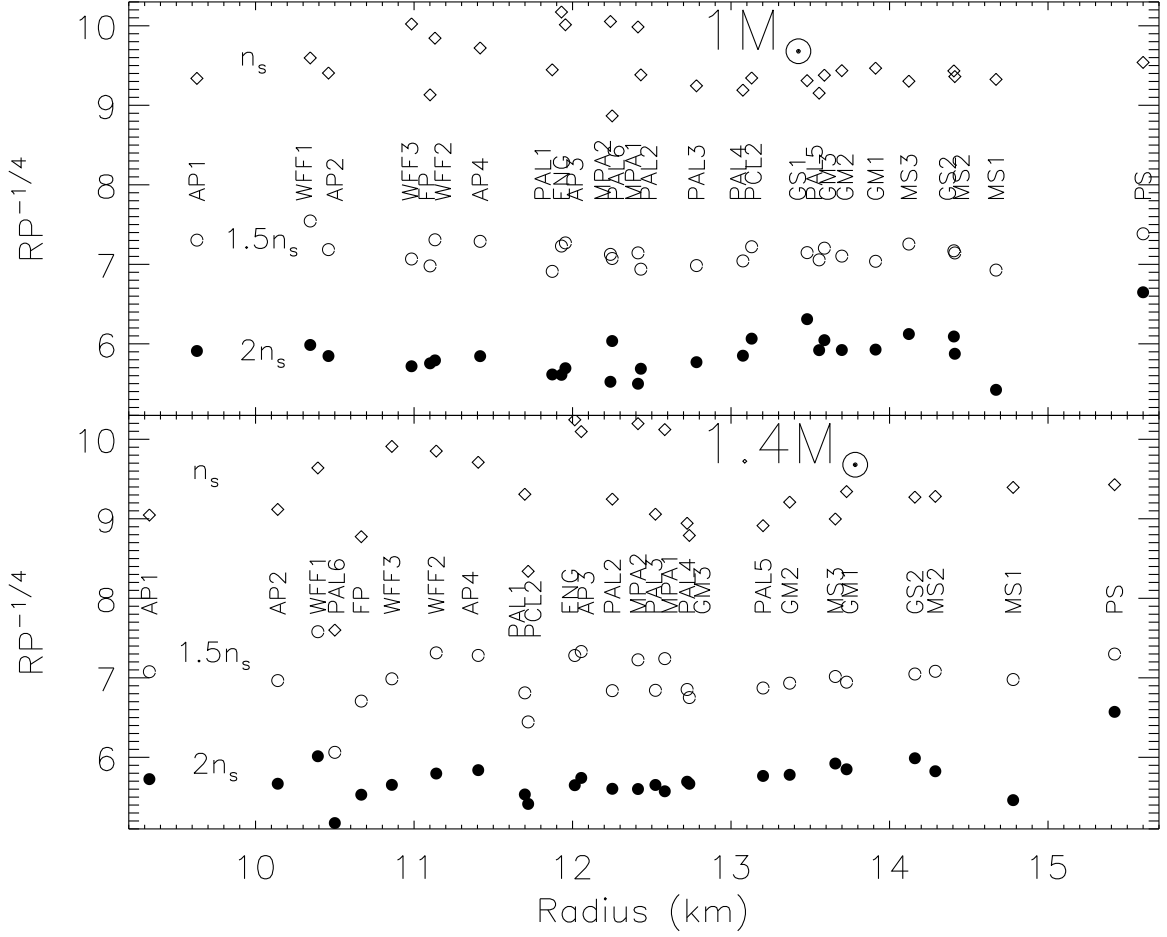


Fig. 3.— Empirical relation between pressure, in units of  $\text{MeV fm}^{-3}$ , and  $R$ , in km, for EOSs listed in Table 1. The upper panel shows results for  $1 M_\odot$  (gravitational mass) stars; the lower panel is for  $1.4 M_\odot$  stars. The different symbols show values of  $RP^{-1/4}$  evaluated at three fiducial densities.

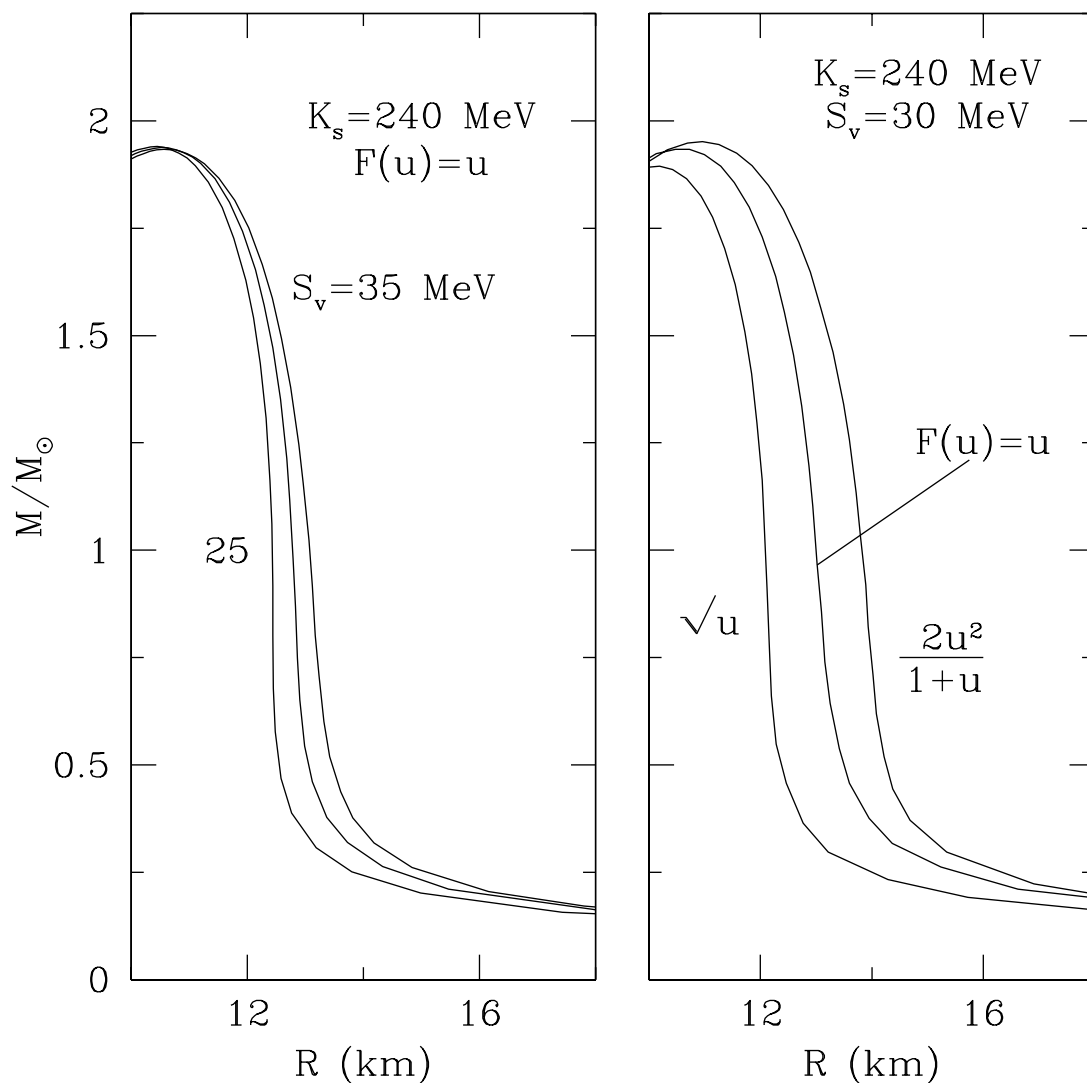


Fig. 4.— Left panel: Mass-radius curves for selected PAL (Prakash, Ainsworth & Lattimer 1988) forces showing the sensitivity to symmetry energy. The left panel shows variations arising from different choices of  $S_v$ , the symmetry energy evaluated at  $n_s$ ; the right panel shows variations arising from different choices of  $S_v(n)$ , the density dependent symmetry energy. In this figure, the shorthand  $u = n/n_s$  is used.

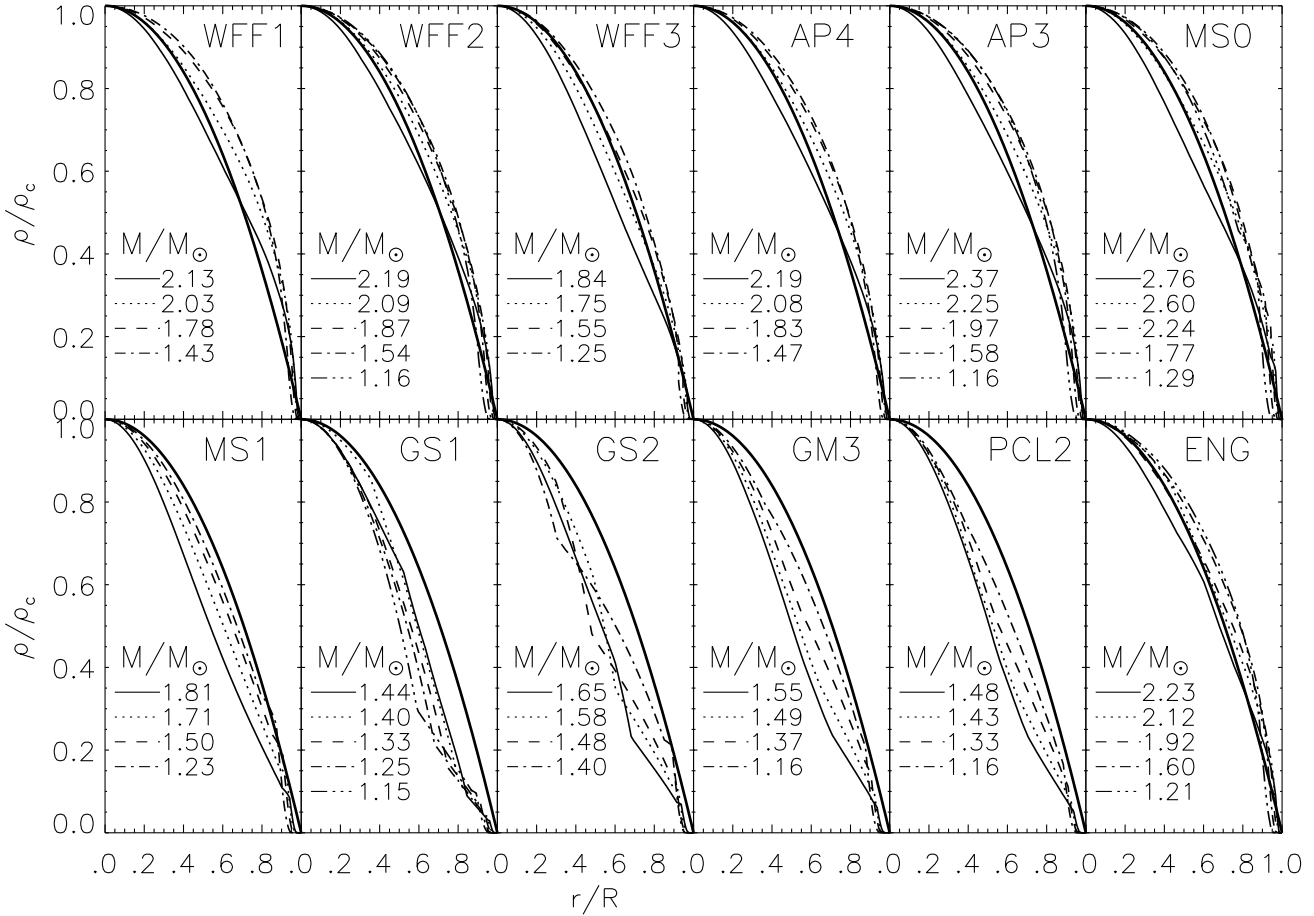


Fig. 5.— Profiles of mass-energy density ( $\rho$ ), relative to central values ( $\rho_c$ ), in neutron stars for several EOSs listed in Table 1. For reference, the thick black lines show the simple quadratic approximation  $1 - (r/R)^2$ .

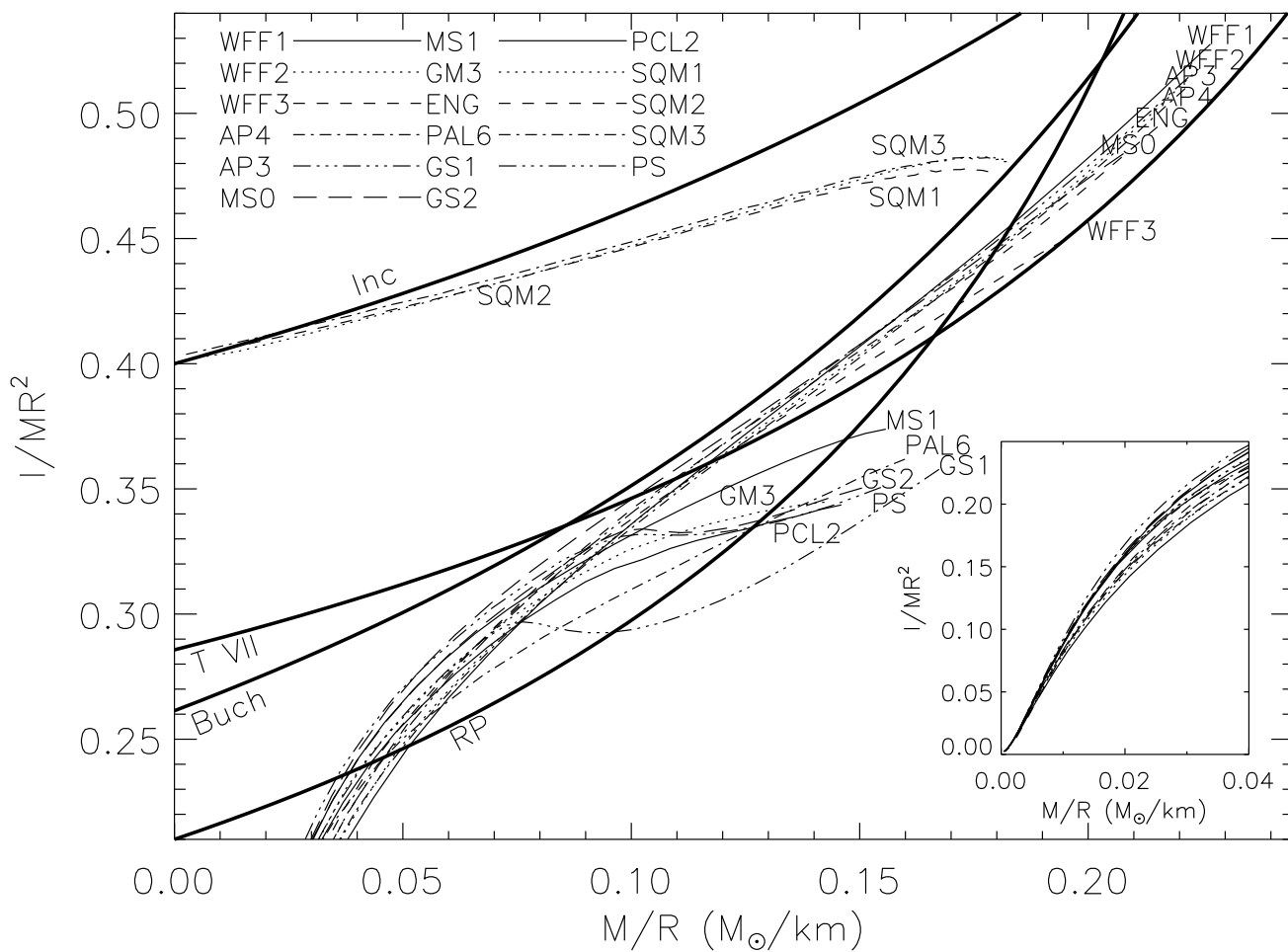


Fig. 6.— The moment of inertia  $I$ , in units of  $MR^2$ , for several EOSs listed in Table 1. The curves labelled “Inc”, “T VII”, “Buch” and “RP” are for an incompressible fluid, the Tolman (1939) VII solution, the Buchdahl (1967) solution, and an approximation of Ravenhall & Pethick (1994), respectively. The inset shows details of  $I/MR^2$  for  $M/R \rightarrow 0$ .

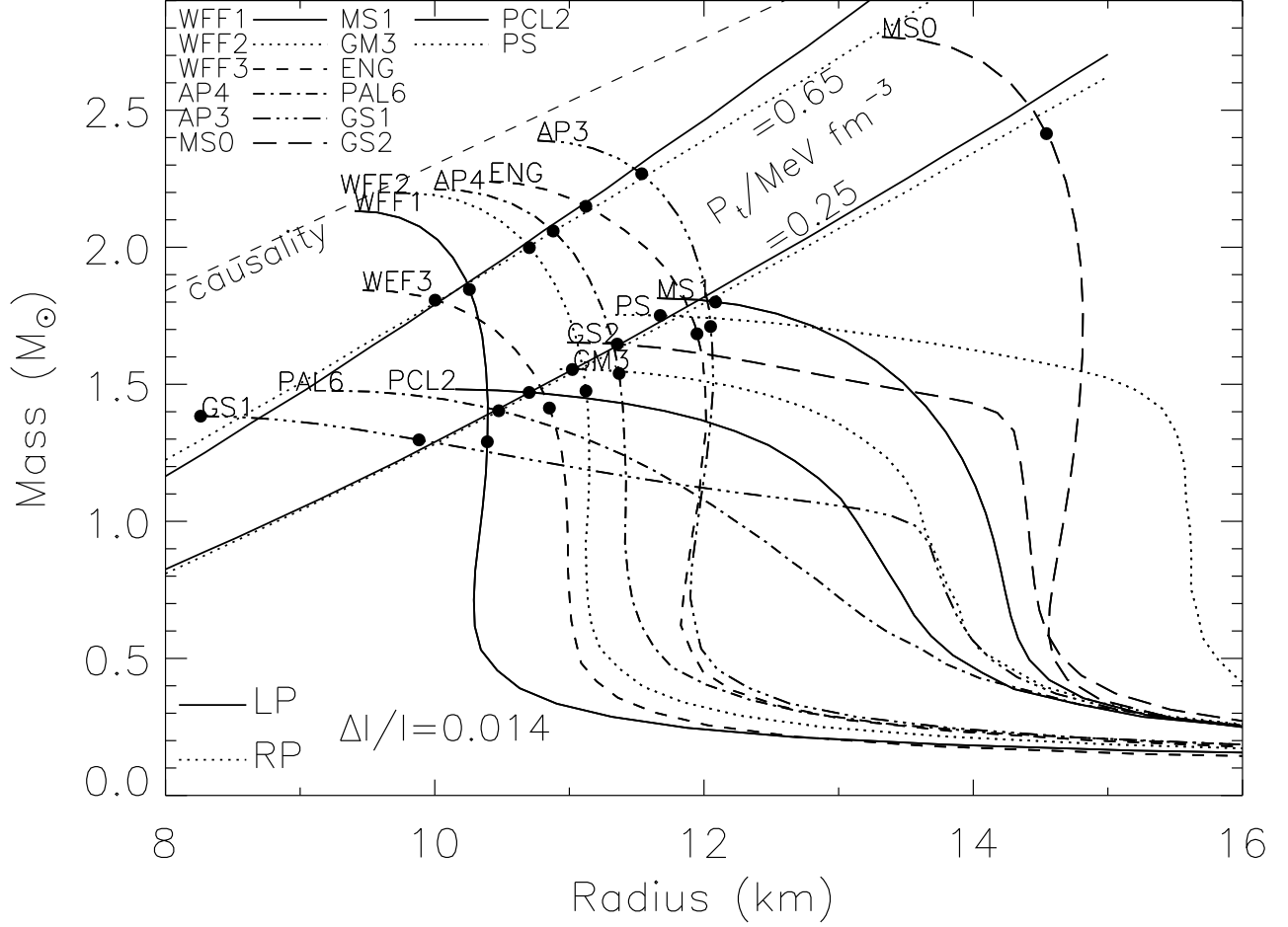


Fig. 7.— Mass-radius curves for selected EOSs from Table 1, comparing theoretical contours of  $\Delta I/I = 0.014$  from approximations developed in this paper, labelled “LP”, and from Ravenhall & Pethick (1994), labelled “RP”, to numerical results (solid dots). Two values of  $P_t$ , the transition pressure demarking the crust’s inner boundary, which bracket estimates in the literature, are employed. The region to the left of the  $P_t = 0.65 \text{ MeV fm}^{-3}$  curve is forbidden if Vela glitches are due to angular momentum transfers between the crust and core, as discussed in Link, Epstein & Lattimer (1999). For comparison, the region excluded by causality alone lies to the left of the dashed curve labelled “causality” as determined by Lattimer et al. (1990) and Glendenning (1992).



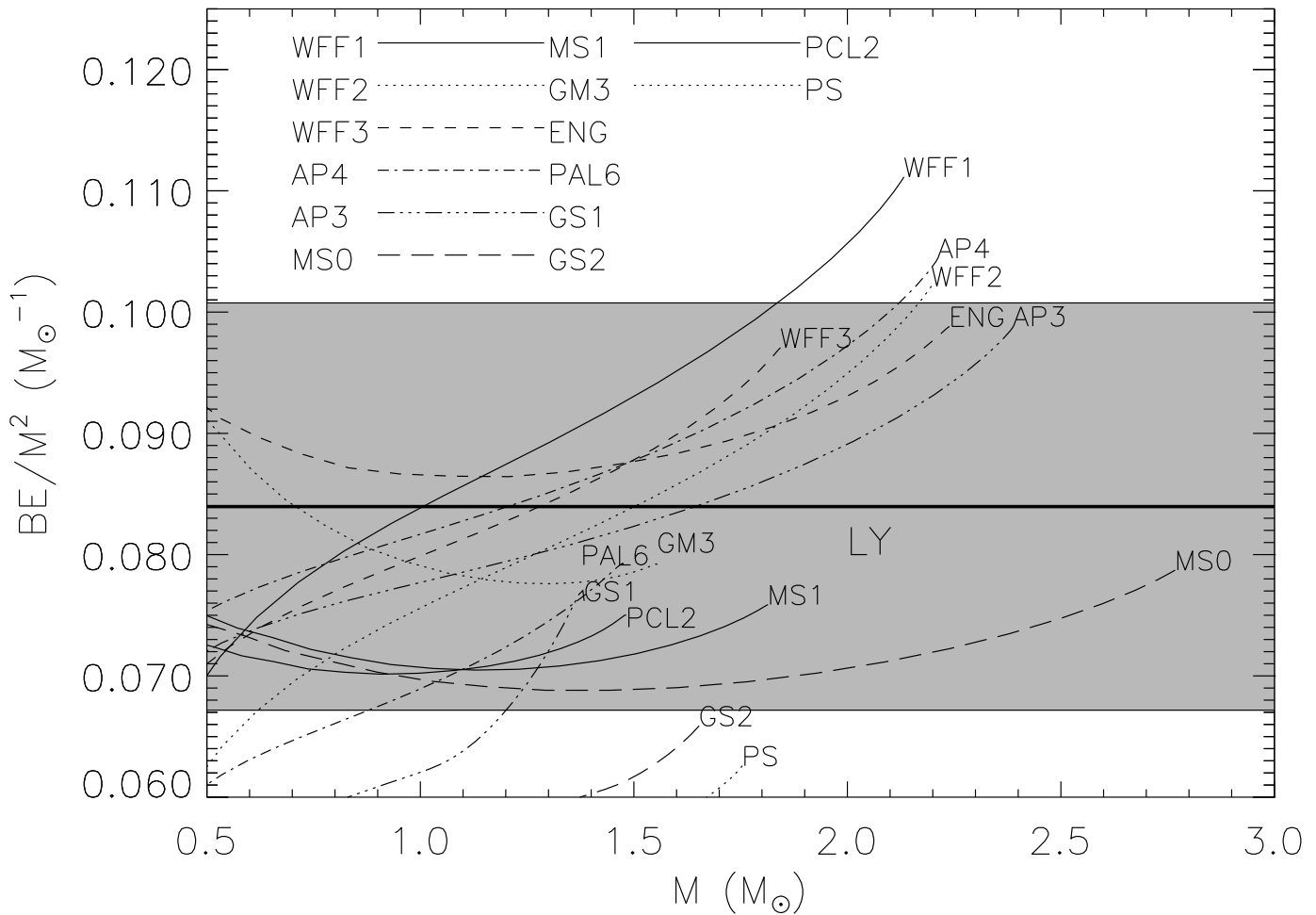


Fig. 8.— The binding energy of neutron stars as a function of stellar gravitational mass for several EOSs listed in Table 1. The predictions of equation (32), due to Lattimer & Yahil (1989), are shown by the line labelled “LY” and the shaded region.

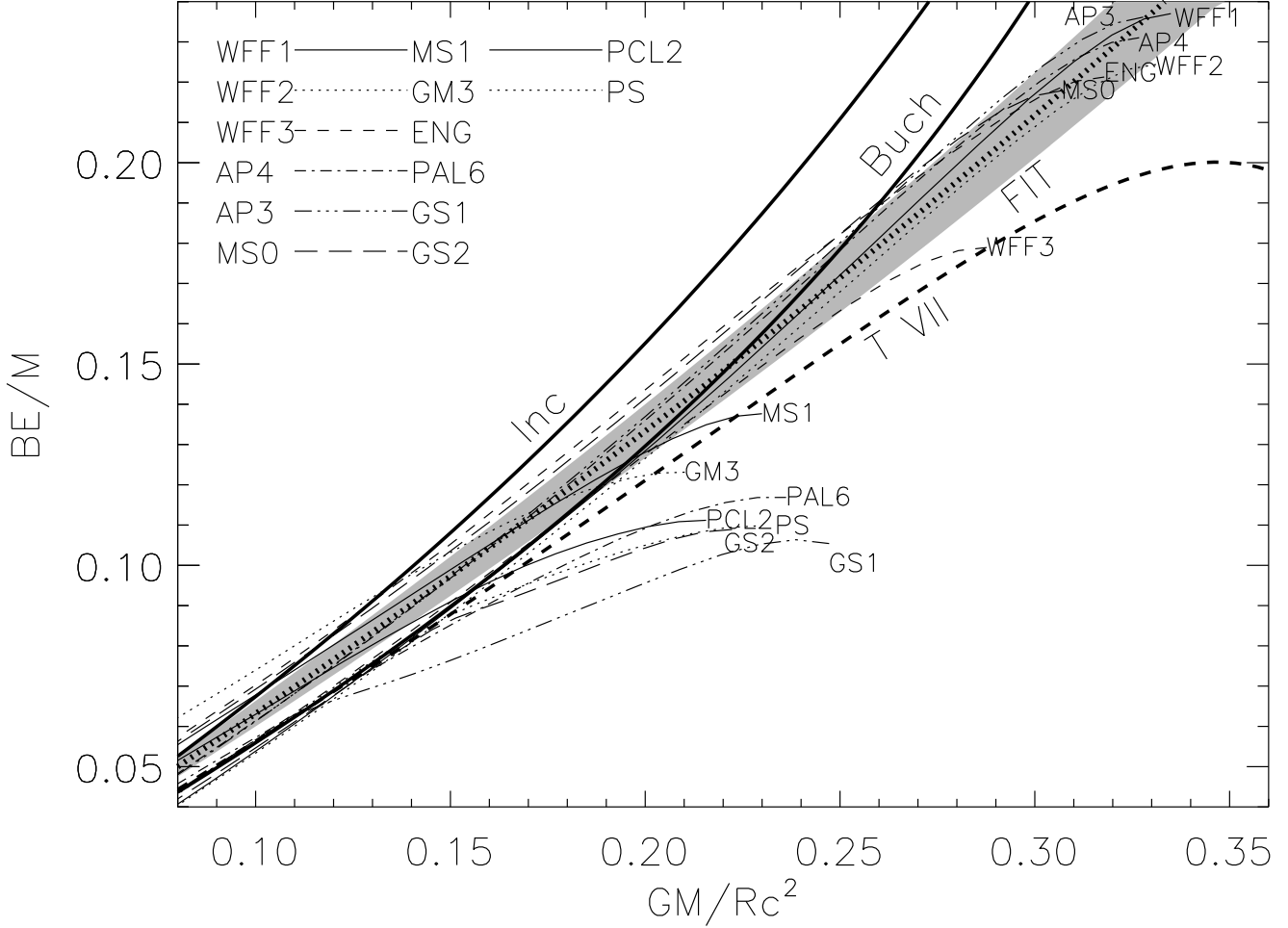


Fig. 9.— The binding energy per unit gravitational mass as a function of compactness ( $\beta = GM/Rc^2$ ) for several EOSs listed in Table 1. Solid lines labelled “Inc”, “Buch” and “T VII” show predictions for an incompressible fluid, the solution of Buchdahl (1967), and the Tolman (1939) VII solution, respectively. The dotted curve and shaded region labelled “FIT” is the approximation given by equation (33).

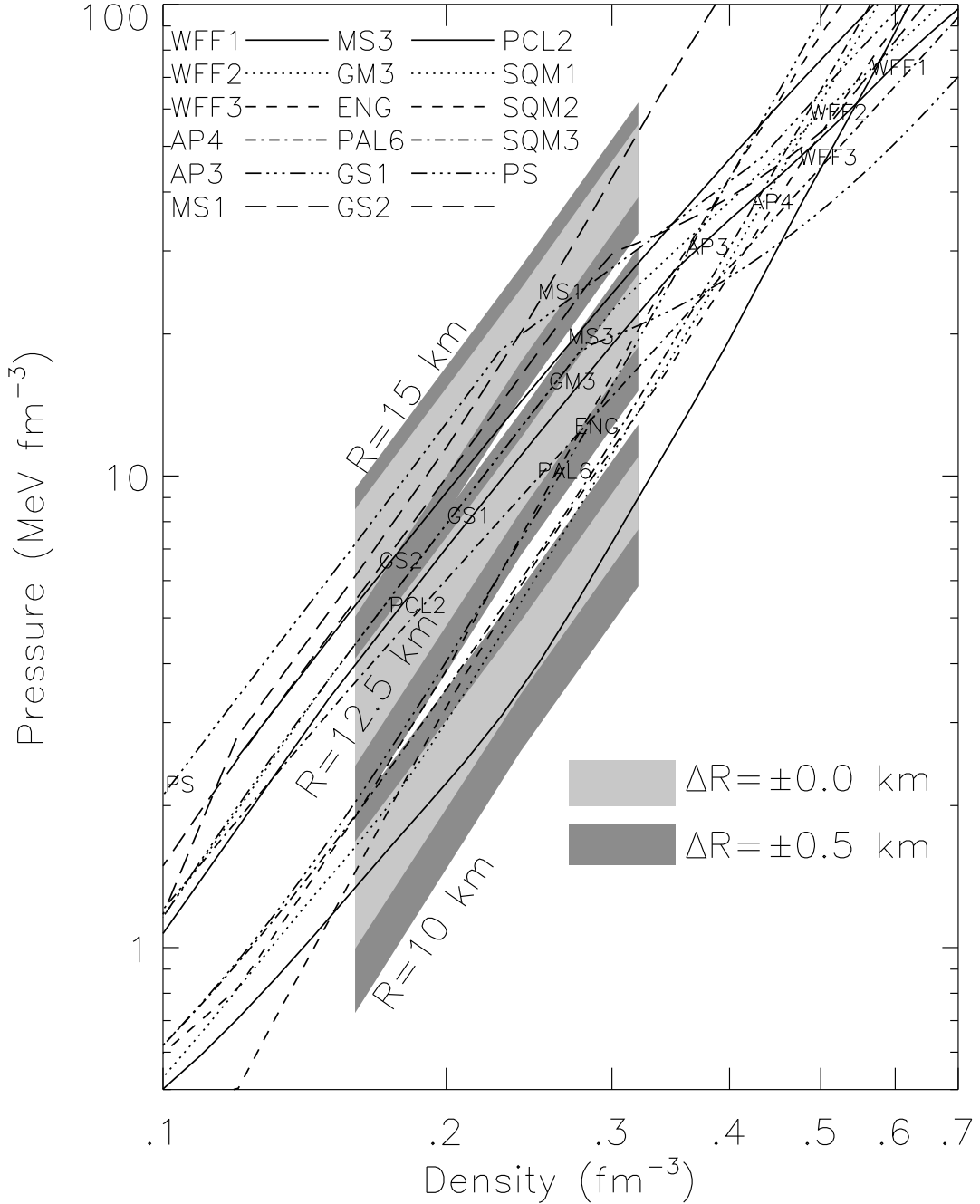


Fig. 10.— The pressures inferred from the empirical correlation equation (5), for three hypothetical radius values (10, 12.5 and 15 km) overlaid on the pressure-density relations shown in Figure 1. The light shaded region takes into account only the uncertainty associated with  $C(n, M)$ ; the dark shaded region also includes a hypothetical uncertainty of 0.5 km in the radius measurement. The neutron star mass was assumed to be  $1.4 M_{\odot}$ .